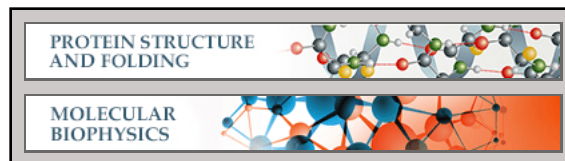


Protein Structure and Folding:
**Conserved distal loop residues in the
Hsp104 and ClpB middle domain contact
nucleotide-binding domain 2 and enable
Hsp70-dependent protein disaggregation**



Morgan E. Desantis, Elizabeth A. Sweeny,
David Snead, Eunice H. Leung, Michelle S.
Go, Kushol Gupta, Petra Wendler and James
Shorter
J. Biol. Chem. published online November 26, 2013

Access the most updated version of this article at doi: [10.1074/jbc.M113.520759](https://doi.org/10.1074/jbc.M113.520759)

Find articles, minireviews, Reflections and Classics on similar topics on the [JBC Affinity Sites](#).

Alerts:

- [When this article is cited](#)
- [When a correction for this article is posted](#)

[Click here](#) to choose from all of JBC's e-mail alerts

This article cites 0 references, 0 of which can be accessed free at
<http://www.jbc.org/content/early/2013/11/26/jbc.M113.520759.full.html#ref-list-1>

Conserved distal loop residues in the Hsp104 and ClpB middle domain contact nucleotide-binding domain 2 and enable Hsp70-dependent protein disaggregation.

Morgan E. DeSantis^{1,2}, Elizabeth A. Sweeny^{1,2}, David Snead^{1,3}, Eunice H. Leung^{1,4}, Michelle S. Go^{1,5}, Kushol Gupta¹, Petra Wendler⁶, and James Shorter^{1,2}

¹From the Department of Biochemistry and Biophysics, ²Biochemistry and Molecular Biophysics Graduate Group, Perelman School of Medicine, University of Pennsylvania, Philadelphia, PA 19104, U.S.A. ³Present address: Department of Biochemistry, Weill Cornell Medical College, New York, NY 10065, U.S.A. ⁴Present address: Li Ka Shing Faculty of Medicine, The University of Hong Kong, Pokfulam, Hong Kong, China. ⁵Present address: University of Illinois College of Medicine at Peoria, One Illini Drive, Peoria, IL 61605, U.S.A. ⁶Gene Center, Department of Biochemistry, Ludwig-Maximilians-Universität München, Feodor-Lynen-Strasse 25, 81377 München, Germany.

*Running title: Hsp104 distal loop enables collaboration with Hsp70

To whom correspondence should be addressed: James Shorter, 805B Stellar-Chance Laboratories, 422 Curie Boulevard, Philadelphia, PA 19104. U.S.A. Phone: 215-573-4256; Fax: 215-898-9871; E-mail: jshorter@mail.med.upenn.edu

Key words: Hsp104, Hsp70, ClpB, DnaK, disaggregase

Background: How Hsp104 and ClpB co-ordinate polypeptide handover with Hsp70 to dissolve disordered protein aggregates is unknown.

Results: Conserved distal loop residues in the Hsp104 and ClpB middle domain contact NBD2 and enable Hsp70-dependent protein disaggregation.

Conclusion: Distal loop does not project out into solution and Hsp104 and ClpB are tuned differently for Hsp70 collaboration.

Significance: Understanding how protein disaggregases operate may empower strategies to counter protein-misfolding disorders.

ABSTRACT

The homologous hexameric AAA+ proteins, Hsp104 from yeast and ClpB from bacteria, collaborate with Hsp70 to dissolve disordered protein aggregates but employ distinct mechanisms of intersubunit collaboration. How Hsp104 and ClpB co-ordinate polypeptide handover with Hsp70 is not understood. Here, we define conserved distal loop residues between middle domain (MD) helix 1 and 2 that are unexpectedly critical for Hsp104 and ClpB collaboration with Hsp70. Surprisingly, the Hsp104 and ClpB MD distal loop does not contact Hsp70 but makes intra-subunit contacts with nucleotide-binding

domain 2 (NBD2). Thus, the MD does not invariably project out into solution as in one structural model of Hsp104 and ClpB hexamers. These intra-subunit contacts as well as those between MD helix 2 and NBD1 are different in Hsp104 and ClpB. NBD2-MD contacts dampen disaggregase activity and must separate for protein disaggregation. We demonstrate that ClpB requires DnaK more stringently than Hsp104 requires Hsp70 for protein disaggregation. Thus, we reveal key differences in how Hsp104 and ClpB co-ordinate polypeptide handover with Hsp70, which likely reflects differential tuning for yeast and bacterial proteostasis.

Our structural and mechanistic understanding of how the homologous hexameric AAA+ ATPases, Hsp104 and ClpB, disaggregate diverse substrates is limited (1,2). Hsp104 in *Saccharomyces cerevisiae* and ClpB in *Escherichia coli* confer tolerance to thermal and chemical stress by rescuing proteins trapped in disordered aggregates (3-7). Hsp104 orthologues in other fungi, bacteria, and plants perform similar roles (8-11). Like many AAA+ proteins, Hsp104 and ClpB form ring-shaped hexamers with a central channel (12,13). Each monomer contains an N-terminal domain, two AAA+ domains that bind and hydrolyze ATP (NBD1 and NBD2), and

a coiled-coil middle domain (MD) inserted in NBD1 (Fig. 1A, B) (1,2,14). Hsp104 has a C-terminal extension not found in ClpB, which is critical for Hsp104 hexamerization (Fig. 1A) (15).

Hsp104 and ClpB are often assumed to share a common mechanism of action due to high sequence homology in their NBDs and because some Hsp104-ClpB chimeras retain partial disaggregase activity (16-20). Hsp104 and ClpB couple energy from ATP hydrolysis to disordered aggregate dissolution, which proceeds via partial or complete translocation of substrate through the central channel of the hexamer (16,17,21-25). However, several dissimilarities suggest that Hsp104 and ClpB hexamers are tuned differently (2,26). For instance, ADP or ATP binding to NBD1 is critical for ClpB hexamerization (27), whereas ADP or ATP binding to NBD2 is critical for Hsp104 to hexamerize (12,28,29). Furthermore, NBD1 contributes the majority of basal ATPase activity in Hsp104 (28-31), whereas both NBDs contribute in ClpB (27). ClpB and Hsp104 display differential sensitivity to activation or inhibition of disaggregase activity by the slowly hydrolysable ATP analog, ATP γ S, and by mutant subunits defective in ATP hydrolysis and substrate binding (26,32). These differences confer Hsp104 with the plasticity needed to rapidly disassemble highly stable, cross- β amyloid and prion fibrils, as well as their toxic oligomeric precursors, whereas ClpB has limited activity against these substrates (26,33-37). These dissimilarities suggest mechanistic differences in how Hsp104 and ClpB disaggregate proteins that we are only beginning to comprehend.

Hsp104 and ClpB usually require cofactors to dissolve disordered aggregates (2). Exceptions, however, abound. Thus, ClpB from *Thermus thermophilus* and *Ehrlichia chaffeensis* disaggregate disordered aggregates without cofactors (38,39) and Hsp104 disaggregates diverse amyloids without cofactors (26). Typically, however, to dissolve disordered aggregates Hsp104 and ClpB must collaborate with the Hsp70 chaperone system: Hsp70 (DnaK in *E. coli*) and its obligate co-chaperone Hsp40 (DnaJ in *E. coli*) (5,6,40), or be provided with permissive ratios of ATP γ S:ATP (~5:1-1:3 ATP γ S:ATP) in vitro (26,32,41). ATP γ S is thought to co-ordinate ATP hydrolysis in a way

that enables Hsp104 and ClpB to dissolve disordered aggregates without Hsp70 (32,41). Thus, permissive ATP γ S:ATP ratios allow the disaggregation of disordered aggregates by Hsp104 or ClpB to be studied in the absence of Hsp70 (32,41). This, in turn, allows mutations to be defined in Hsp104 or ClpB that specifically ablate Hsp70 collaboration but do not affect the intrinsic disaggregase activity of Hsp104 or ClpB. By intrinsic disaggregase activity we mean disaggregase activity observed in the absence of Hsp70 but in the presence of ATP γ S:ATP or in the presence of ATP alone.

Precisely how Hsp70 and Hsp104 coordinate substrate handling in protein disaggregation is unclear (42). Hsp104 cannot collaborate with bacterial DnaK and ClpB cannot collaborate with eukaryotic Hsp70 (2,5,18-20,43). Hsp70 and DnaJ collaborate with Hsp104, whereas DnaK and Hsp40 cannot (5). Thus, Hsp70 determines specificity and might interact with Hsp104 directly (44-46).

The coiled-coil MD of Hsp104 and ClpB plays a key role in Hsp70 collaboration (18-20) and is comprised of four helices (Fig. 1B, C). Artificial Hsp104 chimeras containing the ClpB MD (in place of the Hsp104 MD) weakly collaborate with DnaK to disaggregate disordered aggregates, whereas artificial ClpB chimeras containing the Hsp104 MD can interface with eukaryotic Hsp70 (18-20). Transplanting artificial chimeric MDs into ClpB suggested that helices 2 and 3 of the ClpB MD are critical for DnaK collaboration, whereas helix 4 is not and helix 1 plays an important but not critical role (2,19). By contrast, helices 1, 2, and 3 of the Hsp104 MD are important for collaboration with eukaryotic Hsp70 (2,19). Portions of helix 2 and 3 (amino acids 481 to 500) of the ClpB MD might transiently engage Hsp70 directly (44,45). Moreover, specific mutations in helix 2 and 3 of ClpB (e.g. Y503A) abolished ClpB collaboration with DnaK (44,47,48). A more N-terminal stretch of MD helix 2 of Hsp104 (amino acids 477-488) transiently engages Hsp70 and replacing three lysines (K480, K481, and K482) in this region with glutamate or alanine ablates Hsp104 disaggregase activity in the presence of Hsp70 (46).

Here, we build on previous studies and define the function and location of the distal loop

region (residues 430–446) between helix 1 and 2 of the MD of Hsp104 (Fig. 1B-D). The function of the MD distal loop has been largely ignored and its location in the hexamer remains controversial due to radically different placements in conflicting hexameric models of Hsp104 and ClpB (14,48-50). Indeed, there is no high-resolution structure of Hsp104 or ClpB hexamers, and two conflicting models have been proposed based on cryo-electron microscopy (EM) studies (2,14,49-52). Here, we uncover several Hsp104 variants with mutations in the MD distal loop that retain WT intrinsic disaggregase activity (i.e. are activated by ATP γ S:ATP and inactive with ATP alone without Hsp70) but are unable to collaborate with Hsp70. This distal loop function is conserved and enables ClpB collaboration with DnaK. We show that the distal loop does not stably contact Hsp70, but regulates Hsp104 and ClpB activity via an autoinhibitory intramolecular contact with NBD2. This NBD2-MD contact is inconsistent with structural models of ClpB and Hsp104 hexamers in which the distal loop projects out into solution away from the hexamer (14,46,49,53) or invariably contacts NBD1 of the neighboring subunit (48). We establish that ClpB requires DnaK more stringently than Hsp104 requires Hsp70 to dissolve disordered aggregates. Thus, we reveal a crucial unanticipated role for the MD distal loop of Hsp104 and ClpB in Hsp70 collaboration, as well as unexpected differences in how these protein disaggregases dissolve disordered aggregates.

Experimental Procedures

Protein expression and purification

ClpB and Hsp104 mutants were generated via QuikChange Lightning mutagenesis (Agilent). ClpB variants were expressed as C-terminally His₆-tagged constructs from a pDS56/RBSII plasmid in M15 cells (Qiagen). Hsp104 variants, including isolated MD (amino acids 407-527) were expressed and purified as N-terminally His₆-tagged constructs (54) or as untagged constructs. Briefly, Hsp104 in pNOTAG (31) was transformed into BL21-DE3 RIL cells (Agilent). Expression was induced at an OD₆₀₀ of 0.4-0.6 with 1mM IPTG for 15-18h at 15°C. Cells were harvested via centrifugation (4,000 rpm, 4°C, 20min), resuspended in lysis buffer (50mM

TrisHCl, pH 8, 10mM MgCl₂, 2.5% glycerol (w/v), 2mM β -mercaptoethanol, 5 μ M pepstatin, and 1 Mini-EDTA free protease tabs per 50ml [Roche]), and lysed via treatment with 20mg of Hen Egg Lysozyme per 1l of cells followed by probe sonication. Cell debris was removed via centrifugation at 16,000 rpm at 4°C. The supernatant was applied to 3ml Affi-Gel Blue (Bio-Rad) per 1l of cell culture. Supernatant and resin were rotated at 20rpm at 4°C for 3h. Resin was then washed 4 times with wash buffer (50mM TrisHCl, pH 8, 10mM MgCl₂, 100mM KCl, 2.5% glycerol [w/v], 2mM β -mercaptoethanol). Hsp104 was eluted with high-salt buffer (wash buffer with 1M KCl). Hsp104 was then purified further by Resource Q anion-exchange chromatography and size-exclusion chromatography (54). The isolated MD (amino acids 407-527) was cloned into a derivative of pET DUET (55) to yield a N-terminally GST-tagged MD (GST-MD). This construct was transformed into BL21-DE3 RIL cells, which were grown until mid-log phase and then induced with 1mM IPTG for 2.5h at 37°C. GST-MD was purified using glutathione-sepharose according to manufacturer's instructions (GE). Firefly luciferase was from Sigma. Hsc70, Hdj2, DnaK, DnaJ, and GrpE were from Enzo Life Sciences. Unless otherwise stated, ClpB and Hsp104 concentrations refer to the hexamer.

Luciferase Reactivation

Luciferase reactivation was performed as described (5). To assemble aggregates, firefly luciferase (50 μ M) in luciferase refolding buffer (LRB: 25mM HEPES-KOH pH 7.4, 150mM KAOc, 10mM MgAOc, 10mM DTT) with 6M urea was incubated at 30°C for 30min. The sample was then rapidly diluted 100-fold into LRB, divided into 100 μ l aliquots, snap frozen in liquid N₂, and stored at -80°C. For reactivation assays, aggregated luciferase (50nM) was incubated with Hsp104 (1 μ M), Hsc70 (1 μ M) and Hdj2 (1 μ M) plus ATP (5.1mM) and an ATP regeneration system (1mM creatine phosphate, 0.25 μ M creatine kinase [Roche]) for 90min at 25°C. In some experiments, Hsc70 and Hdj2 were replaced with 4mM ATP γ S and 1.1mM ATP. In other experiments, isolated His₆-MD (6 μ M or 36 μ M) was added. For luciferase reactivation by ClpB, Hsp104, Hsc70, and Hdj2 were replaced with

ClpB (0.167 μ M), DnaK (0.167 μ M), DnaJ (0.033 μ M) and GrpE (0.0167 μ M) and the reaction was incubated for 60min at 25°C. In some experiments, DnaK, DnaJ, and GrpE were replaced by 2.5mM ATP γ S and 2.6mM ATP. For experiments with disulfide-crosslinked Hsp104 or ClpB variants, luciferase aggregates were assembled and reactivated as above except that DTT was omitted from all buffers. Luciferase activity was assessed with a luciferase assay system (Promega). Luminescence was monitored on a Tecan Safire² or Infinite M1000 plate reader. For doping experiments, the conditions for ClpB and Hsp104 were kept as similar as possible. Thus, GrpE was present (0.167 μ M) or absent from the reaction and 1 μ M ClpB, 1 μ M DnaK, and 1 μ M DnaJ were used. Hsp104, Hsc70, and Hdj2 were used as described above. Total Hsp104 or ClpB was comprised of WT or mutant or a 1:5, 2:4, 3:3, 4:2, 5:1 mixture of the two. To ensure statistical subunit mixing, WT and mutant Hsp104 or ClpB mixtures were equilibrated for 15min on ice prior to addition to the reaction (26).

In Vivo Thermotolerance Assay

W303 Δ *hsp104* (*MATa*, *can1-100*, *his3-11,15*, *leu2-3,112*, *trp1-1*, *ura3-1*, *ade2-1*, *hsp104:kanMX4*) yeast were transformed with a centromeric plasmid bearing the *HSP104* promoter, pHSE, or pHSE encoding Hsp104 or the indicated Hsp104 variant (4). Strains were grown in SD-ura media to an OD₆₀₀ of 0.55 and then incubated at 37°C for 30min to induce Hsp104 variant expression. Cells were then heat shocked at 50°C for 0-20min. After heat shock, cells were transferred to ice for 2min and spotted on SD-ura in a 5-fold dilution series. Plates were incubated at 30°C for 2 days. Alternatively, cells were plated onto SD-ura and allowed to recover for 3 days at 30°C to assess viability. Colonies were counted using an aCOLyte automated colony counter (Synbiosis). Immunoblot showed that each Hsp104 protein was expressed at similar levels.

Circular Dichroism (CD)

Hsp104 variants were dialyzed into CD buffer (50mM Na₃PO₄, 50mM K₃PO₄, and 10mM MgAOc, pH 7) and the concentration was adjusted to 1 μ M monomer. Data were collected on an Aviv Biomedical Inc. CD spectrophotometer (Mode

410). Samples were scanned from 260nm-190nm with a 1nm step-size and a 15s averaging time at 25°C.

Size Exclusion Chromatography (SEC)

Hsp104 variants were exchanged into running buffer (RB; 40mM HEPES-KOH pH 7.4, 150mM KCl, 10mM MgCl₂, and 1mM DTT). Hsp104 concentration was adjusted to 35 μ M monomer and 100 μ l of sample was fractionated by a Superose 6 10/300 column (GE).

ATPase Assay

Hsp104 or ClpB (0.25 μ M monomer) were incubated for 12min at 25°C (for Hsp104) or 30min at 25°C (for ClpB) with ATP (1mM). ATPase activity was determined by the amount of inorganic phosphate released using a malachite green phosphate detection kit (Innova).

Hsp70 Pull-down with GST-MD

GST or GST-MD was coupled to glutathione-sepharose at 2.5 μ g/ μ l and incubated for 15min on ice with Hsc70 (3.5 μ M) in storage buffer (40mM HEPES pH 7.4, 150mM KCl, 20mM MgCl₂, 10% glycerol (w/v), 1mM DTT). Recovered beads were washed 4 times in storage buffer, with the second wash containing 1mM ATP, and then eluted with storage buffer plus 20mM reduced glutathione. Samples were processed for SDS-PAGE and Coomassie staining.

Tryptophan Fluorescence

Hsp104 variants were dialyzed into Low Salt Buffer (20mM HEPES-KOH pH 7.4, 20mM NaCl, 10mM MgCl₂, 1mM DTT) to ensure that all proteins were hexameric, even in the absence of nucleotide (30). Concentration was adjusted to 5.5 μ M monomer and samples were left in the apo state or incubated with 5mM ATP, ADP, ATP γ S, or AMP-PNP (a non-hydrolysable ATP analog). Samples were excited at 295nm (4mm bandwidth) and emission was collected from 305-505nm (3nm bandwidth) with a 1nm step size using a Fluorolog-3-21 Jobin-Yvon Spex Instrument SA (Edison, NJ). Spectra of buffer matched controls were subtracted.

X-ray Footprinting

WT Hsp104 was purified as above except

the final step of purification was gel filtration using a Superdex 200 column (GE) equilibrated in 50mM sodium cacodylate pH 7.0, 140mM KCl, and 10mM MgCl₂. Hsp104 was diluted immediately prior to use to 10μM in 50mM sodium cacodylate pH 7.0, 140mM KCl, 10mM MgCl₂, supplemented with 1mM ADP or ATPγS (for the hexamer). Oxidation of Alexa 488 (Invitrogen) was used to determine optimal exposure time for each buffer and provide normalization constants. Samples were exposed to a mirror-focused synchrotron x-ray beam (5.5mrad angle, focus value or 6mm) at the X28C beamline of the National Synchrotron Light Source at Brookhaven National Laboratory for 0-20ms. Exposure time was controlled by flow rate through the flow cell of a KinTek (Austin, TX) stopped flow apparatus (56). Oxidation was immediately quenched with methioninamide (10mM) and samples were snap frozen in liquid N₂. Irradiated protein samples were thawed on ice, diluted to 1μM in 5mM HEPES NaOH pH 7.0, 140mM KCl, 10mM MgCl₂, 1mM DTT, 1% TFA, and injected into an on-line fragmentation-separation/MS analysis system. Samples passed through an immobilized pepsin column onto a C18 trap column. Following a 3min wash, peptides were eluted with a non-linear elution gradient optimized for the highly charged Hsp104 peptide fragments (6μl/min non-linear 2-50% acetonitrile gradient with 0.1% formic acid at pH 2 and 0°C) and passed through an analytical C18 HPLC column before injection by electron spray ionization (ESI) to an LTQ Orbitrap XL mass spectrometer (Thermo Scientific). To enhance peptide identification, selected peptide ions (the four most abundant in each scan) were fragmented by CID and measured in the LTQ stage. A “peptide pool” of unmodified peptides was obtained by combining high probability peptides identified from 0ms MS runs. A program used for the identification of H/D exchange data, ExMS (57), was modified to identify oxidatively modified peptides. A list of theoretical modified peptides was created using the unmodified peptide pool and the list of potential modifications for each amino acid (58), and the MS spectra was searched for the theoretical masses. Results were confirmed by searching the spectra with a modified ExMS (57) analysis against the Hsp104 primary sequence.

The fraction of unmodified peptide was calculated by taking the intensity of the unmodified peak over the sum of the unmodified peptide and all singly modified versions of the peptide. Data were fit to a first order exponential to determine the rate of modification, which was then normalized using the Alexa488 decay data.

Disulfide and 1,4-bis-maleimidobutane (BMB) crosslinking

For crosslinking, we employed an Hsp104 variant, Hsp104^{6CS}, where all six of Hsp104's native cysteines (positions: 209, 400, 643, 718, 721, and 876) are mutated to serine. Engineered cysteines were introduced into this background. For ClpB, native cysteines were not mutated to serine. After purification, samples were exchanged into RB without DTT. Protein concentrations were adjusted to 60μM and samples were incubated with 1mM diamide for 30min at room temperature. Samples were exchanged into RB without DTT to remove excess diamide. Disulfide crosslink formation was assessed via SDS-PAGE on 4-20% Tris-HCl non-reducing gel in comparison to non-crosslinked samples (BioRad). Gels were Coomassie stained and intramolecular disulfide formation caused proteins to migrate more slowly (47). Quantification of band intensities was determined by densitometry. In some cases, Ellman's Reagent (Thermo Scientific Pierce) was used to quantify the amount of free-sulfhydryls and thus disulfide formation according to manufacturer's instructions. In other experiments, the flexible 11Å crosslinker BMB was used to make a covalent intramolecular crosslink between A430C to F630C in Hsp104^{6CS:A430C:F630C} according to manufacturer's instructions (Thermo Scientific Pierce). For all activity assays with disulfide crosslinked proteins, DTT was omitted unless specifically stated.

Small-Angle and Wide-Angle X-Ray Scattering (SAXS and WAXS)

SAXS and WAXS data were collected simultaneously at beamline X9 at the National Synchrotron Light Source (NSLS, Upton, NY) at 10°C by two overlapping detectors, a Mar 165 CCD SAXS detector 3.4m from the sample, and a custom built Photonic Science CCD WAXS detector. The two-dimensional scattering images

collected on the CCD detectors were circularly averaged using software developed at the beamline to yield one-dimensional scattering profiles as a function of momentum transfer q ($q=4\pi\sin(\theta)/\lambda$, where 2π is the scattering angle and λ is the wavelength). The x-ray wavelength was 0.855Å and the angular range collected was $0.00550 \leq Q \leq 1.0060$. The sample cell contained a glass capillary sealed across the evacuated chamber. Protein samples and matching buffer solutions were flowed through the capillary during exposure to reduce radiation damage. For data collection, 30µl of the protein sample at concentrations between 1.5-6mg/ml or matching buffer (20mM Hepes-KOH, pH 7.4, 140mM KCl, 10mM MgCl₂, 2mM DTT, 2mM ATP) was exposed for 180s, subdivided into three 60s exposures of 10µl. After each measurement the capillary was washed thoroughly and purged with compressed nitrogen.

The raw scattering data were scaled and buffer subtracted using the program PRIMUS (59). Each individual scattering curve was visually inspected for radiation damage and aggregation prior to averaging, including Guinier and Kratky plot analysis. Averaged scattering curves from the SAXS and WAXS detectors were scaled and merged in PRIMUS to yield a low-noise composite curve. The radii of gyration (R_g) were initially calculated using Guinier plots (60). $P(r)$ distance distribution functions were calculated by the program GNOM (61) using an indirect Fourier transform. The maximum dimension of the particle (D_{max}) was determined by examining the quality of fit to the experimental data for a D_{max} range of 180Å to 280Å, varied in 5Å increments. Fits were performed to maximize the Total Estimate figure, to minimize the discrepancy between calculated and experimental profiles, and to optimize the visual properties of the shape distribution function. Values for R_g were computed from the second moment of the $P(r)$ and compared favorably to those calculated using Guinier plots.

Mathematical modeling of heterohexamer ensemble activity

We simulated the distribution of WT and mutant subunits within a given population of Hsp104 or ClpB hexamers as described (26). Briefly, we employed the binomial distribution:

$$P(x) = \binom{n}{x} p^x (1-p)^{n-x}$$

where P is the probability that a hexamer (thus, $n=6$) contains x mutant subunits and p is the probability that a mutant subunit is incorporated. Experiments demonstrated that mutant and WT subunits have a similar probability of being incorporated into a hexamer (26). Consequently, p is calculated as the molar ratio of mutant and WT protein present:

$$p = \frac{Hsp104_{mut}}{(Hsp104_{mut} + Hsp104_{WT})}$$

Therefore, for any specified percentage of mutant subunits the probability distribution of Hsp104 hexamers containing 0, 1, 2, 3, 4, 5 or 6 mutant subunits can be derived (Fig. 9A). Activity versus p plots (Fig. 9B) could then be generated assuming each WT subunit makes an equal contribution to the total activity (one-sixth per subunit). Consequently, if subunits within the hexamer operate independently then activity should decline in a linear manner upon incorporation of defective mutant subunits. Conversely, if subunits are coupled then a specific number of subunits will be sufficient to eliminate activity. Thus, zero activity is assigned to hexamers that are in breach of a specific threshold number of mutant subunits. In this way, we can generate activity versus p plots if we assume that 1 or more, 2 or more, 3 or more, 4 or more, or 5 or more mutant subunits are required to eliminate activity (26,38).

Results

The Y507A mutation in Hsp104 has pleiotropic effects on disaggregase functionality

First, we assessed the MD helix 3 variant, Hsp104^{Y507A} (Fig. 1C) in induced thermotolerance in yeast (4). Hsp104^{Y507A} is the equivalent of ClpB^{Y503A}, which is specifically defective in DnaK collaboration (44,47). In preconditioned $\Delta hsp104$ cells, Hsp104^{Y507A} provided limited thermotolerance (Fig. 2A). After 20min at 50°C, Hsp104^{Y507A} conferred survival levels similar to the vector control (Fig. 2A). However, Hsp104^{Y507A} was not completely inactive and after 10min at 50°C provided significant thermotolerance similar to WT Hsp104 (Fig. 2A).

WT Hsp104 and Hsp104^{Y507A} were expressed at similar levels (data not shown). Hsp104^{Y507A} reactivated aggregated luciferase *in vivo* although not as effectively as WT Hsp104 (Fig. 2B). Thus, contrary to expectations from data obtained with ClpB^{Y503A} (44,47), Hsp104^{Y507A} is hypomorphic and not a null variant.

Can Hsp104^{Y507A} collaborate with Hsp70? To answer this question, we assessed the ability of Hsp104^{Y507A} to reactivate urea-denatured luciferase aggregates *in vitro* (5). In the presence of Hsp70 and Hsp40, Hsp104^{Y507A} was ~70% as active as WT Hsp104 under the same conditions (Fig. 2C). This finding explains why Hsp104^{Y507A} is partially active *in vivo* (Fig. 2A, B). However, Hsp104^{Y507A} was also highly active in the presence of ATP in the absence of Hsp70 and Hsp40, whereas WT Hsp104 was inactive (Fig. 2C). In the presence of ATP, Hsp70 and Hsp40 only modestly stimulated (~10%) Hsp104^{Y507A} disaggregase activity (Fig. 2C). Moreover, substituting a permissive ratio of ATP γ S:ATP in place of Hsp70 and Hsp40 inhibited Hsp104^{Y507A}, whereas WT Hsp104 was activated (Fig. 2C). Thus, the Y507A mutation is pleiotropic and causes alterations in the intrinsic disaggregase activity of Hsp104 as well as reduced ability to collaborate with Hsp70.

By contrast, ClpB^{Y503A} is selectively impaired in the ability to collaborate with DnaK, DnaJ, and GrpE (KJE). ClpB^{Y503A} has minimal activity in the presence of ATP and absence of DnaK, DnaJ, and GrpE (44,47), and is activated to WT levels with a permissive ratio of ATP:ATP γ S (Fig. 2D). Note that the relative activation of ClpB by ATP:ATP γ S is low compared to ClpB activity in the presence of DnaK, DnaJ, and GrpE (Fig. 2D), whereas in Hsp104 it is considerably higher (Fig. 2C). Thus, for optimal activity ClpB requires Hsp70 more stringently than Hsp104. These findings indicate that mutation of the conserved tyrosine in helix 3 of the MD (Y503 in ClpB, Y507 in Hsp104) to alanine has different functional consequences for Hsp104 versus ClpB.

Specific mutations in the distal loop of Hsp104 selectively ablate Hsp70 collaboration

We sought non-pleiotropic mutations in Hsp104 that specifically ablated collaboration with Hsp70 while having no effect on the intrinsic disaggregase activity of Hsp104 against disordered

aggregates. Such Hsp104 variants would be unable to disaggregate disordered aggregates in the presence of Hsp70 and Hsp40. However, they would still disaggregate disordered aggregates in the presence of ATP γ S:ATP alone and be inactive with ATP alone without Hsp70. We hypothesized that the distal loop (residues 430–446 in Hsp104) between helix 1 and 2 of the MD (Fig. 1C) might be important for Hsp70 collaboration since in another Hsp100, ClpC, this region contacts cofactors (62). Moreover, in peptide arrays, Hsp70 interacts with a peptide (residues 435–448) in this region (46). Thus, we mutated various residues in the distal loop and assessed functionality (Fig. 1C, D).

We focused on three distal loop residues: A430, L431, and D438, because they are highly conserved (Fig. 1B–D). Initially, we made a drastic change and introduced the bulky, hydrophobic residue, tryptophan, in an effort to perturb function. Importantly, CD revealed that Hsp104^{A430W}, Hsp104^{L431W}, and Hsp104^{D438W} were very similar to WT Hsp104 in terms of secondary structure (data not shown). Moreover, the isolated MD bearing the A430W mutation had similar secondary structure to WT MD (data not shown). Hsp104^{A430W}, Hsp104^{L431W}, and Hsp104^{D438W} assembled into hexamers just like WT Hsp104 (data not shown). Thus, these mutations do not grossly perturb Hsp104 structure.

Hsp104^{A430W} and Hsp104^{D438W} retained WT levels of intrinsic disaggregase activity in the presence of a permissive ATP γ S:ATP ratio (Fig. 3A). Intriguingly, Hsp104^{L431W} displayed elevated intrinsic disaggregase activity with ATP γ S:ATP (Fig. 3A). Moreover, like WT Hsp104, these Hsp104 variants possessed no disaggregase activity in the presence of ATP and absence of Hsp70 and Hsp40 (Fig. 3B). Thus, in contrast to Hsp104^{Y507A}, in the absence of Hsp70 the distal loop variants Hsp104^{A430W}, Hsp104^{A430Y}, and Hsp104^{D438W} are activated by ATP γ S:ATP and inactive with ATP alone similar to WT Hsp104.

In striking contrast to WT Hsp104, Hsp104^{A430W}, Hsp104^{L431W}, and Hsp104^{D438W} were unable to collaborate with Hsp70 and Hsp40 to reactivate aggregated luciferase (Fig. 3C). Indeed, in the presence of Hsp70 and Hsp40 plus ATP, Hsp104^{A430W}, Hsp104^{L431W}, and Hsp104^{D438W} were completely inactive (Fig. 3C). We obtained similar

results when we substituted these positions with tyrosine instead of tryptophan (Fig. 3A-C). Hsp104^{A430Y} and Hsp104^{D438Y} retained WT or levels of intrinsic disaggregase activity in the presence of ATP γ S:ATP, whereas Hsp104^{A431Y} disaggregase activity with ATP γ S:ATP was elevated (Fig. 3A). Moreover, Hsp104^{A430Y}, Hsp104^{A431Y}, and Hsp104^{D438Y} were completely inactive in the presence of ATP alone (Fig. 3B), or when combined with Hsp70 and Hsp40 (Fig. 3C). These are the first Hsp104 mutants that are: (a) unable to collaborate with Hsp70 and Hsp40; (b) inactive with ATP alone; and (c) retain disaggregase activity elicited by ATP γ S:ATP. Thus, conserved MD distal loop residues are critical for Hsp70 collaboration.

Conserved distal loop residues regulate Hsp104 disaggregase activity

Next, we explored the effect of different missense mutations at position A430 (Fig. 1C, D) on intrinsic disaggregase activity and ability to collaborate with Hsp70 and Hsp40. Interestingly, Hsp104^{A430D} and Hsp104^{A430L} displayed reduced disaggregase activity elicited by ATP γ S:ATP (Fig. 3A) and reduced Hsp70-dependent disaggregation (Fig. 3C). By contrast, Hsp104^{A430V} was active in the presence of Hsp70 and Hsp40 (Fig. 3C), and was also slightly active in the presence of ATP alone (~2.3% of WT-Hsp104 with Hsp70 and Hsp40; Fig. 3B). However, Hsp104^{A430V} had lost intrinsic disaggregase activity in the presence of ATP γ S:ATP (Fig. 3A). Thus, depending upon the precise substitution, mutation of A430 can inhibit Hsp70 collaboration (e.g. W), inhibit intrinsic disaggregase activity in the presence of ATP γ S:ATP (e.g. V), or both (e.g. D or L). These findings suggest that A430 plays a key role in regulating Hsp104 disaggregase activity.

We next explored different missense mutations at L431 (Fig. 1C), which is highly conserved (Fig. 1D). Against disordered luciferase aggregates, Hsp104^{L431A} displayed lowered activity in Hsp70-dependent disaggregation (Fig. 3C) and Hsp70-independent disaggregation elicited by ATP γ S:ATP (Fig. 3A). The reduction was more severe for intrinsic disaggregase activity elicited by ATP γ S:ATP (Fig. 3A, C). By contrast, Hsp104^{L431D} displayed mildly reduced Hsp70-dependent disaggregase activity (Fig. 3C),

whereas the intrinsic disaggregase activity in the presence of ATP γ S:ATP was not significantly affected (Fig. 3A). Interestingly, Hsp104^{L431D} exhibited some ability to reactivate aggregated luciferase with ATP alone in the absence of Hsp70 and Hsp104 (~12.2% of WT-Hsp104 with Hsp70 and Hsp40), whereas WT Hsp104 is completely inactive under these conditions (Fig. 3B). Thus, L431 also regulates Hsp104 disaggregase activity.

We also explored D438 variants (Fig. 1C). Mutation of D438 to W, Y, L, or A had the same effect: Hsp70-dependent reactivation of aggregated luciferase was ablated, whereas intrinsic disaggregase activity in the presence of ATP γ S:ATP or ATP alone was unaltered (Fig. 3A-C). Thus, D438 plays a critical role in Hsp70 collaboration, but can be substituted and not affect the ability of Hsp104 to process aggregated substrates per se. These studies suggest that A430, L431, and D438 all make important contributions to Hsp70 collaboration. Moreover, A430 and L431 tightly regulate Hsp104 disaggregase activity.

Hsp104^{A430W}, Hsp104^{L431W}, and Hsp104^{D438W} are defective in induced thermotolerance in vivo

We focused on the tryptophan variants: Hsp104^{A430W}, Hsp104^{L431W}, and Hsp104^{D438W}, because they are specifically defective in Hsp70 collaboration (Fig. 3A-C). We tested whether these Hsp104 variants could confer induced thermotolerance in vivo. In preconditioned Δ hsp104 cells, Hsp104^{A430W}, Hsp104^{L431W}, and Hsp104^{D438W} were severely defective in thermotolerance (Fig. 3D, E). Indeed, Hsp104^{A430W} and Hsp104^{L431W} were completely inactive and conferred thermotolerance levels comparable to the vector control (Fig. 3D, E). By contrast, Hsp104^{D438W} afforded some thermotolerance, but was greatly impaired compared to WT Hsp104 (Fig. 3E). Importantly, tryptophan substitutions in the distal loop or elsewhere in the MD did not impair thermotolerance: Hsp104^{A437W}, Hsp104^{A453W}, Hsp104^{Y466W}, Hsp104^{Y497W}, and Hsp104^{Y507W} (Fig. 1C) all conferred thermotolerance comparable to WT Hsp104 (Fig. 3D) (63). Thus, the inability of Hsp104^{A430W}, Hsp104^{L431W}, and Hsp104^{D438W} to confer thermotolerance was a specific effect of tryptophan substitution at precise positions in the distal loop. These Hsp104 variants were expressed

at similar levels (data not shown). Thus, conserved residues in the MD distal loop of Hsp104 enable collaboration with Hsp70 and induced thermotolerance in vivo.

ClpB^{A428W} is unable to collaborate with DnaK

To test conservation in ClpB, we generated ClpB^{A428W}, which is analogous to Hsp104^{A430W} (Fig. 1D). The intrinsic disaggregase activity of ClpB^{A428W} was similar to WT ClpB. Indeed, ClpB^{A428W} was slightly more active than WT ClpB in reactivating aggregated luciferase in the presence of ATP γ S and ATP (Fig. 3F) and inactive in the presence of ATP (Fig. 3G). However, ClpB^{A428W} was unable to collaborate with DnaK, DnaJ, and GrpE (Fig. 3H). Thus, the A428W mutation specifically ablates ClpB-DnaK collaboration. These data suggest that the function of the MD distal loop in Hsp70 collaboration is conserved across two billion years of evolution.

Why are specific Hsp104 distal loop variants selectively impaired in Hsp70 collaboration?

The inability of specific Hsp104 distal loop variants, e.g. Hsp104^{A430W}, Hsp104^{L431W}, and Hsp104^{D438W}, to collaborate with Hsp70 could have at least three causes: (a) these distal loop variants may have an impaired ATPase cycle that precludes collaboration with Hsp70. Indeed, some ATPase-defective ClpB variants are less able to synergize with DnaK (41); (b) by analogy with the ClpC distal loop, which directly engages MecA (62), the distal loop of Hsp104 might directly interact with Hsp70 and facilitate collaboration. Mutations in this region could disrupt an Hsp70-MD interface and impair collaboration; (c) mutations in the distal loop might alter an intramolecular Hsp104 interface that regulates Hsp70 collaboration. In fact, one hexameric model of Hsp104 and ClpB posits that the distal loop lies in close proximity to NBD2 (2,50-52). Thus, mutations in the distal loop may interfere with NBD2-MD contacts in a way that selectively precludes Hsp70 collaboration.

Reduced ATPase activity does not readily explain inability to collaborate with Hsp70

We determined the ATPase activity of each Hsp104 distal loop mutant, as well as WT ClpB and ClpB^{A428W} (Fig. 4A). The majority of

Hsp104 distal loop mutants had mildly impaired ATPase activity, ranging from ~30% (Hsp104^{L431D}: $\sim 3.04 \pm 0.5 \text{ min}^{-1}$) to ~85% (Hsp104^{D438A}: $\sim 11.2 \pm 0.96 \text{ min}^{-1}$) of WT Hsp104 activity ($\sim 13.1 \pm 0.93 \text{ min}^{-1}$). In fact, impairment was statistically significant with the exception of Hsp104^{D438A} (Fig. 4A). Thus, at first glance, impaired ATPase activity of these mutants might explain defective collaboration with Hsp70 (Fig. 4A). However, upon closer inspection there is no simple linear correlation between ATPase activity and ability to collaborate with Hsp70 (Fig. 4B, linear regression $R^2=0.1994$). For example, Hsp104^{D438A} has ~85% WT Hsp104 ATPase activity, but is unable to collaborate with Hsp70 (Fig. 4B), whereas Hsp104^{L431D} has the lowest ATPase activity but can collaborate with Hsp70 in luciferase reactivation (Fig. 3C, 4B). Moreover, ClpB^{A428W}, which is unable to collaborate with DnaK (Fig. 3H), did not have lower ATPase activity than WT ClpB (compare $\sim 3.2 \pm 0.57 \text{ min}^{-1}$ for WT ClpB to $\sim 3.4 \pm 0.06 \text{ min}^{-1}$ for ClpB^{A428W}; Fig. 4A). In fact, if simply decreasing ATPase activity led to defective Hsp70 collaboration, we would expect all distal loop variants to be deficient in Hsp70 collaboration. However, this is not the case. For example, Hsp104^{A430W} can collaborate effectively with Hsp70 (Fig. 3C, 4B). Thus, the moderately impaired ATPase activity of these distal loop variants does not explain their inability to collaborate with Hsp70.

There was also no simple linear relationship between Hsp104 variant ATPase activity and ability to reactivate luciferase in the presence of ATP γ S and ATP (Fig. 4C, linear regression $R^2=0.012$). Thus, the ATPase activity of these Hsp104 variants provides little information about their disaggregase activity in the presence of Hsp70 or ATP γ S and ATP.

Isolated MD does not interact with Hsp70 or inhibit disaggregation in trans

Another possibility for how specific distal loop mutations impair Hsp70 collaboration is that mutation in this region disrupts a direct interaction between this region of Hsp104 and Hsp70. Indeed, in peptide arrays Hsp70 interacts with a distal loop peptide (residues 435-448) in this region (46). However, a direct interaction between this region of Hsp104 and Hsp70 could not be observed using

a crosslinking strategy (46). To test for a direct interaction, we purified isolated Hsp104 MD as a N-terminally GST-tagged protein. We immobilized the Hsp104 MD on glutathione-sepharose and probed for a direct interaction with Hsp70 by affinity chromatography. We were unable to detect an interaction between the Hsp104 MD and Hsp70 (data not shown). Thus, the isolated Hsp104 MD does not appear to form a stable interaction with Hsp70. We may have failed to detect the putative interaction between the Hsp104 MD and Hsp70 because the interaction is too weak or too transient. Thus, we tested whether isolated Hsp104 MD might competitively inhibit the collaboration between Hsp70 and Hsp104 in trans. However, even a 100-fold molar excess of isolated Hsp104 MD had no effect on Hsp70-dependent disaggregation of luciferase by Hsp104 (data not shown). These experiments do not exclude the possibility that the MD of Hsp104 interacts directly with Hsp70. However, the isolated MD appears insufficient to recapitulate the Hsp104 and Hsp70 interaction.

Tryptophan fluorescence reveals that the Hsp104 distal loop is partially buried

Next, we considered the third possibility for why distal loop mutation impairs Hsp70 collaboration. Mutations in the distal loop might alter an intramolecular Hsp104 interface that regulates Hsp70 collaboration. There is no atomic resolution structure of Hsp104, but the monomeric structure of ClpB from *T. thermophilus* has been solved (14). Yet, how monomers pack to form a hexamer is controversial and two conflicting models of Hsp104 hexamer structure have been advanced based on cryo-EM reconstructions (2,14,49-53). In one of these, the MD projects out into solution away from the hexamer (2,14,49,53). In this model, the distal loop appears poorly positioned to make intramolecular contacts with other domains of Hsp104 (2,14,49,53). However in the second model, the MD contacts both NBDs and the distal loop could make an intramolecular contact with NBD2 (2,50-52).

To assess the positioning of the MD within the Hsp104 hexamer, we exploited the fact that Hsp104 has no natural tryptophans, which makes it well suited for site-specific tryptophan fluorescence spectroscopy. This sensitive

technique measures the polarity of microenvironment within 10Å of a Trp residue (64,65). Red-shifted emission maxima (~350nm) indicate a polar microenvironment, e.g. solvated regions, whereas blue shifted emission maxima (~330nm) indicate a more hydrophobic environment, e.g. regions that are shielded from solvent (64,65). We mutated a number of MD residues to tryptophan and determined the fluorescence spectra of each mutant. As controls, we included the Y466 position (Fig. 1C), which is buried in both hexameric models and the Y497 position (Fig. 1C), which is solvated in both models to ensure that we could accurately determine solvation state (49,51,52). Importantly, Hsp104^{Y466W} and Hsp104^{Y497W} confer WT levels of thermotolerance in vivo (Fig. 3D). As expected, in each nucleotide state tested (apo, ADP, ATP, and ATPγS) Hsp104^{Y466W} had blue-shifted emission maxima of ~330nm indicating a buried region, whereas Hsp104^{Y497W} had red-shifted emission maxima of ~350nm, indicating a solvated region (Fig. 5A-D).

Hsp104^{A430W}, Hsp104^{L431W}, and Hsp104^{D438W} exhibited emission maxima between ~335-340nm in each nucleotide state (Fig. 5A-D) indicating that the distal loop is partially shielded from solvent. These findings were not due to studying defective Hsp104 variants because Hsp104^{A437W}, which displays WT levels of thermotolerance (Fig. 3D), also exhibited emission maxima between ~336-339nm (Fig. 5A-D). While fluorescence intensity changed in response to nucleotide for all the distal loop variants, we observed only minor shifts in emission maxima in response to different nucleotides, with the exception of Hsp104^{L431W} where the emission maximum remained at ~335nm for all states (Fig. 5A-D). For example, the emission maximum of Hsp104^{A430W} in the absence of nucleotide and in the presence of ADP was more red-shifted (~339nm and ~338nm, respectively; Fig. 5A, B), whereas the spectra of ATP and ATPγS were more blue-shifted (~337nm; Fig. 5C, D). Likewise, the emission maximum of Hsp104^{D438W} in the presence of ADP was more red-shifted (~341nm; Fig. 5D), whereas in the presence of ATP or ATPγS it was more blue-shifted (~339nm and 340nm, respectively; Fig. 5B, C). While minor, these shifts indicate that A430 and D438 are more

solvated in the apo and ADP states and more buried in the ATP and ATP γ S states.

Tryptophan fluorescence spectra reflect the average of the ensemble of protein conformers. Thus, the intermediate spectra of the distal loop variants can be interpreted in two ways: (1) the distal loop is partially sequestered from solvent all of the time; and (2) the distal loop moves between two different conformations, one of which is solvated and one of which is buried. Hsp104 hexamers are strongly asymmetric with each protomer adopting a distinct conformation (52). Thus, the distal loop could be buried in some subunits but solvent exposed in others. Regardless, the tryptophan emission spectra of Hsp104^{A430W}, Hsp104^{L431W}, Hsp104^{A437W}, and Hsp104^{D438W} indicate that the distal loop is unlikely to always be solvent exposed, which is inconsistent with a model where the MD projects out from the hexamer into solvent in all nucleotide states examined (14,49,53).

X-ray footprinting confirms that distal loop is partially buried

We confirmed that the MD distal loop of Hsp104 was partially buried in WT Hsp104 using synchrotron x-ray mediated hydroxyl radical footprinting, or x-ray footprinting (XF). In XF, milli-second bursts of x-rays generate hydroxyl radicals from solvent molecules (i.e. water). These radicals oxidatively modify solvent exposed protein side chains in well-defined ways, although Ala, Asp, and Asn have lower reactivity and Gly behaves like the main chain (66-68). For very short exposures, solvent-inaccessible regions of the protein are protected from modification (68). Methioninamide HCl is used to stop oxidative modification after exposure (66). Protease digestion of the irradiated sample followed by liquid chromatography electrospray ionization tandem mass spectrometry (MSMS) allows identification of the modified, and thus solvent accessible regions of the protein. Certain nucleotides and buffers can scavenge free radicals and effectively quench oxidative damage. Moreover, high protein concentration or overexposure to x-rays can cause oxidation of protein that does not reflect solvent-accessibility (66,68). To circumvent these issues, Alexa 488, a dye that decreases in fluorescence upon oxidation

by radiolysis, was used to calibrate ideal x-ray dosing conditions for specific Hsp104-nucleotide conditions (67). XF has been successfully used to test structural models of ClpA, a related hexameric AAA+ protein (69).

Having identified ideal x-ray dosing conditions, we exposed Hsp104 to white x-rays for 0-20ms, in the presence of ADP or ATP γ S. Samples were quenched, digested with pepsin, and processed for LC-ESI-MSMS. MSMS-verifiable coverage of pepsin-digested Hsp104 encompassed ~85-90% of the protein. The modification rate of identified peptides was calculated by fitting a first order exponential decay curve extrapolated to zero. The complete XF dataset will be presented elsewhere (E.A.S. & J.S. manuscript in preparation). Here, we tracked a distal loop peptide (residues 431-455) and peptides spanning residues 456-476 that harbor Y466 in helix 2 (Fig. 1C). In agreement with the Hsp104^{Y466W} fluorescence data (Fig. 5C), peptide 456-476 was not modified in the presence of ATP γ S suggesting that this region is solvent inaccessible. In the presence of ADP, peptide 456-466 was modified at time points longer than 2.5ms, whereas peptide 467-474 was unmodified. Although Y466 is predicted to be buried by both models (14,49,51,52), the finding that this entire region (residues 456-476) is protected from modification in ATP γ S is inconsistent with a model of Hsp104 hexamers where the MD projects out from the hexamer into solution (14,49,53).

In the presence of ADP and ATP γ S, the distal loop peptide (residues 431-455) becomes oxidized indicating that it must be partially exposed to solvent (Fig. 5E). The rate of modification is ~7-fold less rapid in ATP γ S (~0.080s⁻¹; Fig. 5E) than in ADP (~0.565s⁻¹; Fig. 5E). Thus, the MD distal loop of WT Hsp104 is less solvent accessible in the presence of ATP γ S and more solvent accessible in the presence of ADP, which is consistent with Hsp104^{A430W} and Hsp104^{D438W} fluorescence (Fig. 5C, D). The MD distal loop of Hsp104 likely shifts from a more buried position to a more solvent exposed position upon ATP hydrolysis. These XF and tryptophan fluorescence data are consistent with a hexameric model in which the MD distal loop is positioned in a way that could make an intramolecular contact with NBD2 (2,50-52).

Engineered disulfides establish that helix 2 and the distal loop of the MD contact NBD2

Using tryptophan fluorescence and XF, we have established that the distal loop of Hsp104 can become shielded from solvent. Size-exclusion chromatography coupled to dynamic light scattering reveal that Hsp104 hexamers are monodisperse in solution (data not shown). Thus, the distal loop of the MD is likely to contact another domain within the Hsp104 hexamer. Where does the distal loop become buried?

To answer this question, we examined an optimized structural model of the Hsp104^{N728A} hexamer in the presence of ATP, where the distal loop is in close proximity to NBD2 (Fig. 5F, G) (50-52). Based upon this optimized model (Fig. 5G), we site-specifically mutated proposed contact residues between MD and NBD2 to cysteine and assessed proximity by attempting to form disulfide crosslinks. This strategy has confirmed that helix 3 of the MD can contact NBD1 in ClpB (14,47). First, however, to avoid confounding effects of the six naturally occurring cysteines in Hsp104, we generated an Hsp104 variant, Hsp104^{6CS}, where all six cysteines are mutated to serine. Hsp104^{6CS} retained approximately WT levels of induced thermotolerance *in vivo* and luciferase disaggregation *in vitro* (data not shown).

We introduced cysteine pairs into the Hsp104^{6CS} background to test the proposed proximity of A430C(MD): F630C(NBD2) (Fig. 6A blue and mauve residues) and K451C(MD): E790C(NBD2) (Fig. 6A, green residues) (50-52). Disulfides were induced by diamide and detected by reduced mobility on non-reducing SDS-PAGE and with Ellman's reagent to quantify free sulfhydryls (47). Single cysteine variants served as negative controls. Disulfide crosslinks readily formed between the MD residue A430C and the NBD2 residue F630C (Fig. 6A, B) as well as between the MD residue K451C and the NBD2 residue E790C (Fig. 6A, C). Both disulfides were intramolecular as no higher order multimeric species were observed in single or double cysteine variants. In both cases, the disulfide formed more readily in the presence of AMP-PNP (a non-hydrolyzable ATP analogue) or ATP than in the presence of ADP (Fig. 6D). Thus, upon ATP binding the distal loop (A430) and helix 2 (K451) of the MD contact NBD2. Upon ATP hydrolysis,

the MD is in less close contact with NBD2, which is in accord with tryptophan fluorescence (Fig. 5C, D) and XF data (Fig. 5E). These findings argue against hexameric models where the MD invariably projects away from the hexamer out into solution (14,49,53) or where the distal loop invariably contacts NBD1 of an adjacent subunit (48), which would both leave the distal loop too distant from NBD2 to form disulfides.

The MD distal loop contacts NBD2 in ClpB

Next, we determined if the NBD2-MD contacts were conserved in ClpB. Thus, we introduced pairs of cysteine residues into ClpB. However, we were unable to form a disulfide between A428C (A430C in Hsp104) and F621C (F630C in Hsp104) in ClpB. By contrast, in ClpB, A428C (Fig. 6E, yellow residue) readily formed a disulfide with L817C (Fig. 6E, orange residue), which is located in the NBD2 small domain (Fig. 6E, F). Unlike Hsp104, we observed maximal disulfide formation in all nucleotide states (Fig. 6F). Thus, the MD is oriented differently in Hsp104 and ClpB. In comparison to Hsp104 the MD of ClpB seems to be rotated ~90° anticlockwise around helix 2. Nonetheless, the MD distal loop also contacts NBD2 in ClpB, which further argues against a hexameric model where the MD invariably projects away from the hexamer out into solution (14,49,53) or where the distal loop invariably contacts NBD1 of an adjacent subunit (48).

NBD1-MD contacts are not conserved between ClpB and Hsp104

The NBD2-MD contacts in Hsp104 and ClpB are not anticipated by a hexameric model of Hsp104 based on the *T. thermophilus* ClpB (tClpB) crystal structure (Fig. 7A) (14,49,53), but are predicted by an Hsp104 cryo-EM model (Fig. 7B) (50-52). This discrepancy prompted us to test whether other engineered disulfides between the MD and NBD1 and within NBD1 of ClpB that were predicted and verified in tClpB could also be formed in Hsp104 (Fig. 7A) (14). Thus, we assessed the following cysteine pairs in Hsp104^{6CS}: I361C(NBD1): K480C(MD) and R366C(NBD1): V540C(NBD1), which correspond to V350C(NBD1): Q467C(MD) (Fig. 7A, B, yellow residues) and R355C(NBD1):

E520C(NBD1) (Fig. 7A, B, light green residues,) in tClpB, respectively (14). I361C(NBD1): K480C(MD) are predicted to form a disulfide in the tClpB model (Fig. 7A, yellow residues), but not the other model (Fig. 7B, yellow residues), whereas R366C(NBD1): V540C(NBD1) are predicted to form a disulfide in both (Fig. 7A, B, light green residues). In agreement with data from tClpB (14), R366C(NBD1): V540C(NBD1) in Hsp104^{6CS} readily formed a disulfide within NBD1 (Fig. 7C, D). Thus, two β -strands of the NBD1 small domain, which are separated in primary sequence by the entire MD, can be linked by a disulfide in Hsp104 and ClpB (14). The crosslink formed extremely effectively in ADP or ATP (Fig. 7C, D). By contrast and as predicted by the Hsp104 cryo-EM model (Fig. 7B) (50-52), disulfides did not form between I361C(NBD1): K480C(MD) in ATP or ADP (Fig. 7C, E). Thus, NBD1-MD domain contacts are not absolutely conserved between ClpB and Hsp104.

Defining NBD1-MD contacts in Hsp104

To define NBD1-MD contacts in Hsp104 we tested predictions from an optimized cryo-EM hexameric model of Hsp104 (Fig. 5G) (50-52). We assessed disulfide formation between K182C(NBD1): E485C(MD) (Fig. 7B, dark blue residues), D247C(NBD1): H471C(MD) (Fig. 7B, cyan residues), D247C(NBD1): E475C(MD) (cyan residues Fig. 7B), and E320C(NBD1): N467C(MD) (Fig. 7B, red residues) in Hsp104^{6CS}. We also assessed H362C(NBD1): D484C(MD) (Fig. 7B, dark green residues), which are not predicted to be in close enough proximity to form disulfides (50-52). Indeed, H362C(NBD1): D484C(MD) did not form disulfides in ATP or ADP (Fig. 7C, F). In the presence of ADP or ATP, K182C(NBD1): E485C(MD), D247C(NBD1): H471C(MD), and D247C(NBD1): E475C(MD) all formed intramolecular disulfides, although the efficiency was ~15-20%, indicating that on average only one subunit per hexamer could make this crosslink (Fig. 7C, G, H, I). By contrast, the E320C(NBD1): N467C(MD) disulfide formed with greater efficiency in ADP (~40%) than ATP (~15%) (Fig. 7C, J). None of these disulfides are expected by a hexameric model where the MD projects out into solution (Fig. 7A) (14,49,53). Thus, upon ATP hydrolysis the MD shifts position

such that A430 in the distal loop moves away from F630 in NBD2 and simultaneously N467 in helix 2 moves closer to E320 of NBD1.

Movement of the MD distal loop away from NBD2 is critical for disaggregation

The crosslinking data suggested that the MD populates two different conformations that result in the distal loop being in two different environments. The first conformation (populated in the ATP-bound state) results in a more solvent-inaccessible distal loop that is juxta-NBD2 and thus able to form a covalent crosslink between the two domains. The second conformation (populated in the ADP-bound state) leaves the distal loop more solvent accessible and not as closely associated with NBD2. To probe the functional importance of the NBD2-MD contact we assessed the luciferase disaggregase and ATPase activity of disulfide-crosslinked and uncrosslinked Hsp104^{6CS:A430C:F630C} and ClpB^{A428C:L817C}. We also crosslinked A430C to F630C in the Hsp104^{6CS} background with the longer and more flexible 11Å linker, BMB. Before crosslinking, Hsp104^{6CS:A430C:F630C} and ClpB^{A428C:L817C} displayed luciferase reactivation levels comparable to WT (Fig. 8A, B, red bars). After disulfide crosslinking, Hsp104^{6CS:A430C:F630C} and ClpB^{A428C:L817C} had very low luciferase reactivation activity, suggesting that the crosslinks nixed disaggregase activity (Fig. 8A, B, blue bars). Importantly, reduction of the Hsp104^{6CS:A430C:F630C} and ClpB^{A428C:L817C} disulfides restored disaggregase activity (Fig. 8A, B, grey bars). Thus, the crosslinking procedure itself does not result in impaired activity. We confirmed by SDS-PAGE that BMB induced an upshift indicative of an intramolecular crosslink in ~85% of total Hsp104^{6CS:A430C:F630C}. In contrast to disulfide-crosslinked Hsp104^{6CS:A430C:F630C}, BMB-crosslinked Hsp104^{6CS:A430C:F630C} retained some disaggregase activity, whereas Hsp104^{6CS} was unaffected (Fig. 8A, green bars). Thus, a longer, more flexible crosslink between NBD2 and the distal loop permits some disaggregase activity.

To determine how the disulfide crosslink between MD and NBD2 inhibits disaggregase activity, we examined the ATPase activity of Hsp104^{6CS:A430C:F630C} and ClpB^{A428C:L817C}. Hsp104^{6CS:A430C:F630C} displayed an elevated ATPase rate (~25±0.67min⁻¹) compared to WT Hsp104

($\sim 13.1 \pm 0.93 \text{ min}^{-1}$) (Fig. 8C, red bar). Disulfide-crosslinked Hsp104^{6CS:A430C:F630C} had reduced ATPase activity ($\sim 9.54 \pm 1.63 \text{ min}^{-1}$) (Fig. 8C, blue bar). Inhibition was relieved upon reduction of the Hsp104^{6CS:A430C:F630C} disulfide ($\sim 27 \pm 0.67 \text{ min}^{-1}$), indicating that the NBD2-MD disulfide contact inhibits ATP hydrolysis (Fig. 8C, grey bar). BMB-crosslinked Hsp104^{6CS:A430C:F630C} was less inhibited ($\sim 15.2 \pm 0.3 \text{ min}^{-1}$) (Fig. 8C, green bar). By contrast, disulfide-crosslinked ClpB^{A428C:L817C} had similar ATPase activity to uncrosslinked ClpB^{A428C:L817C} (Fig. 8D). Thus, in ClpB, constraining the distal loop contact with NBD2 inhibits disaggregase activity (Fig. 8B) without significantly affecting ATPase activity. Collectively, the foregoing data suggest that the distal loop of the MD and NBD2 of the same subunit are in close proximity and can form an autoinhibitory contact that tightly constrains the disaggregase activity of Hsp104 and ClpB. Based on these observations, we suggest that a critical step in the activation of Hsp104 and ClpB for protein disaggregation lies in the separation of these autoinhibitory NBD2-MD contacts.

The A430W mutation changes the shape and compacts the Hsp104 hexamer

To determine how the distal loop mutants might affect Hsp104 hexamer structure, we performed SAXS and WAXS to determine the maximum dimension (D_{max}) and radius of gyration (R_g) of WT Hsp104 and Hsp104^{A430W} hexamers in the presence of ATP (Table 1; Fig. 8E). SAXS exploits the fact that x-ray scattering by a particle at very low angles contains information about particle size and shape. The pairwise distance distribution ($P(r)$ curve), which represents the distances between pairs of atoms within a given volume, reveals that Hsp104^{A430W} has a smaller D_{max} than WT Hsp104 (205 Å compared to 230 Å for WT Hsp104). Moreover, the R_g , which is the root mean square average of all of the interatomic distances with respect to the center-of-mass, is shorter for Hsp104^{A430W} than for WT Hsp104 (compare 64 Å to 68.2 Å) (Table 1; Fig. 8E). Thus, Hsp104^{A430W} occupies a smaller spatial extent in solution than WT Hsp104 (Table 1). The smaller spatial extent of Hsp104^{A430W} is evident in the $P(r)$ curves where WT Hsp104 exhibits a decrease in smaller interatomic vectors near the R_g (the peak

and an increase in larger interatomic vectors (Fig. 8E). The Porod volume of Hsp104^{A430W} is also smaller than that of WT Hsp104 (Table 1). Porod-Debye analysis (70) indicated that large changes in flexibility do not underlie these differences (Porod exponents, P_x , of 3.9 and 3.7 for the WT Hsp104 and Hsp104^{A430W} hexamers, respectively; Table 1). Thus, the A430W mutation likely stabilizes the NBD2-MD contact in a way that yields a more compact hexamer, which occupies a smaller spatial extent and volume and cannot collaborate with Hsp70.

Hsp104 has a less stringent requirement for Hsp70 collaboration than ClpB

Hsp104 and ClpB form dynamic hexamers, which exchange subunits rapidly and randomly. Thus, we can use a mutant-doping strategy to ask how many subunits per hexamer are required for a given aspect of Hsp104 or ClpB activity (26,38). Here, WT subunits are mixed with subunits that contain a mutation that specifically abolishes one aspect of activity (e.g. Hsp70 collaboration). These mixtures rapidly form heterohexamers containing both WT and mutant subunits according to the binomial distribution (Fig. 9A) (26,38). By applying these heterohexamer ensembles to reactivate disordered luciferase aggregates, we obtain a measure of how many WT subunits per hexamer are required for a specific activity (e.g. Hsp70 collaboration) (Fig. 9B). For example, by mixing WT Hsp104 with Hsp104^{A430W} or WT ClpB with ClpB^{A428W} in known and established ratios we were able to determine how many WT subunits per hexamer are required for Hsp104 or ClpB to collaborate with Hsp70 during disaggregation. We conducted doping experiments (see Experimental Procedures) with Hsp104^{A430W} and ClpB^{A428W}. ClpB was more sensitive to the Hsp70-collaboration deficient mutant than Hsp104. In fact, ClpB required between 3 and 4 WT subunits per hexamer to disaggregate luciferase (Fig. 9C, grey markers), while Hsp104 only required 2 WT subunits per hexamer (Fig. 9C, green markers).

We were concerned that the differences observed between Hsp104 and ClpB might be due to GrpE, a nucleotide exchange factor for DnaK, which is included in ClpB-mediated reactivation, but not in the Hsp104 experiments. To determine

if GrpE could account for the observed differences, we repeated the ClpB^{A428W} doping experiments, but omitted GrpE. Here, we observed an even more deleterious effect upon titration of ClpB^{A428W}. In the absence of GrpE, ClpB required between 5 and 6 WT subunits per hexamer to accomplish disaggregation (Fig. 9C, orange markers). Thus, more ClpB subunits per hexamer must be competent to collaborate with Hsp70 than Hsp104 subunits for successful disaggregation. Since these mutant doping studies of *in vitro* luciferase reactivation by Hsp104 and ClpB accurately model physiological conditions (26), we suggest that Hsp104 and ClpB hexamers differ fundamentally in how they collaborate with Hsp70.

Discussion

Here, we establish for the first time that conserved residues in the MD distal loop of Hsp104 and ClpB are specifically critical for collaboration with Hsp70. We establish that the MD distal loop forms an autoinhibitory intrasubunit contact with NBD2, which is consistent with some hexameric models of Hsp104 (50-52), but not others (14,48,49,53). Recently, the MD of Hsp104 and ClpB has been implicated as being crucial for collaboration with Hsp70 (44-46,48). To isolate Hsp104 and ClpB variants specifically defective in Hsp70 collaboration we exploited the fact that Hsp104 and ClpB resolve disordered aggregates in the absence of Hsp70 when supplemented with mixtures of ATP γ S and ATP, and are inactive with ATP alone. Thus, we were able to exclude pleiotropic mutants, such as Hsp104^{Y507A}, which were active with ATP alone in the absence of Hsp70 and Hsp40, and inactive in the presence of ATP γ S and ATP. Introducing W or Y at the highly conserved 430 or 431 position or introducing A, L, W, or Y at the 438 position in Hsp104, specifically ablated Hsp70 collaboration, without activating Hsp104 in the presence of ATP alone or perturbing disaggregase activity in the presence of ATP γ S and ATP. This function of the MD distal loop in Hsp70 collaboration is conserved in ClpB.

Why are some distal loop mutants (e.g. Hsp104^{A430W}, ClpB^{A428W}) unable to collaborate with Hsp70? These mutants form hexamers, retain WT secondary structure, possess robust ATPase

activity, and disaggregate disordered aggregates in the presence of permissive ATP γ S:ATP ratios. The MD distal loop does not engage Hsp70 directly (44-46,48). Rather, it makes intra-subunit contacts with NBD2, which is consistent with one hexameric model of Hsp104 (51,52) but not with models where the MD invariably project out into solution (14,49,53) or where the distal loop invariably contacts NBD1 of the neighboring subunit (48). When the NBDs are populated with ATP or ATP γ S, the distal loop of the MD is less solvent accessible and when ADP is present, the distal loop is more solvent accessible. In Hsp104, upon ATP hydrolysis the MD shifts such that A430 in the distal loop moves away from F630 in NBD2 and at the same time N467 in helix 2 moves into closer proximity with E320 of NBD1. We suggest that the NBD2-MD interface is autoinhibitory and must separate for successful protein disaggregation. Constraining the interface with disulfide crosslinks but not longer BMB crosslinks prevents protein disaggregation in the presence of Hsp70 and Hsp40. Distal loop variants, such as Hsp104^{A430W}, may mimic the disulfide crosslinking effect by stabilizing the distal loop and NBD2 interaction. In fact, Hsp104^{A430W} hexamers are more compact, which may be due to a tighter interaction between the distal loop and NBD2.

We used Hsp104^{A430W} and ClpB^{A428W} in subunit doping experiments (26) to determine how many Hsp70-collaboration competent subunits are required per hexamer to disaggregate disordered substrates. We determined that Hsp104 only requires 2 WT subunits to collaborate with Hsp70, whereas ClpB required between 3 and 4 WT subunits in the presence of GrpE and 5-6 subunits in the absence of GrpE (Fig. 9C). Thus, ClpB has a more rigid requirement for Hsp70 collaboration than Hsp104, and this requirement is intensified in the absence of GrpE. This result was surprising because it indicated that Hsp104 and ClpB differ fundamentally in their mechanism of collaboration with Hsp70. This fundamental difference between Hsp104 and ClpB, defined here with pure components, is likely to explain differences between Hsp104 and ClpB observed under physiological conditions. More ClpB subunits per hexamer must be competent to interact functionally with Hsp70 than Hsp104 subunits.

This distinction likely reflects important differences in how substrate handover from Hsp70 to ClpB and Hsp104 is co-ordinated. For example, more ClpB subunits per hexamer are likely required to wrench substrate from Hsp70, particularly in the absence of GrpE. Moreover, ClpB is more dependent upon Hsp70 for optimal

activity than Hsp104 (Fig. 2C, D). These differences between Hsp104 and ClpB likely reflect differential tuning for the respective challenges of yeast and bacterial proteostasis.

References

1. Barends, T. R., Werbeck, N. D., and Reinstein, J. (2010) Disaggregases in 4 dimensions. *Curr. Opin. Struct. Biol.* **20**, 46-53
2. DeSantis, M. E., and Shorter, J. (2012) The elusive middle domain of Hsp104 and ClpB: location and function. *Biochimica et biophysica acta* **1823**, 29-39
3. Parsell, D. A., Kowal, A. S., Singer, M. A., and Lindquist, S. (1994) Protein disaggregation mediated by heat-shock protein Hsp104. *Nature* **372**, 475-478
4. Sanchez, Y., and Lindquist, S. L. (1990) HSP104 required for induced thermotolerance. *Science* **248**, 1112-1115
5. Glover, J. R., and Lindquist, S. (1998) Hsp104, Hsp70, and Hsp40: A novel chaperone system that rescues previously aggregated proteins. *Cell* **94**, 73-82
6. Goloubinoff, P., Mogk, A., Zvi, A. P., Tomoyasu, T., and Bukau, B. (1999) Sequential mechanism of solubilization and refolding of stable protein aggregates by a bichaperone network. *Proc Natl Acad Sci U S A* **96**, 13732-13737
7. Mogk, A., Tomoyasu, T., Goloubinoff, P., Rudiger, S., Roder, D., Langen, H., and Bukau, B. (1999) Identification of thermolabile *Escherichia coli* proteins: prevention and reversion of aggregation by DnaK and ClpB. *EMBO J.* **18**, 6934-6949
8. Queitsch, C., Hong, S. W., Vierling, E., and Lindquist, S. (2000) Heat shock protein 101 plays a crucial role in thermotolerance in *Arabidopsis*. *The Plant cell* **12**, 479-492
9. Motohashi, K., Watanabe, Y., Yoshida, M., and Yoshida, M. (1999) Heat-inactivated proteins are rescued by the DnaK.J-GrpE set and ClpB chaperones. *Proc. Natl. Acad. Sci. U.S.A.* **96**, 7184-7189
10. Senechal, P., Arseneault, G., Leroux, A., Lindquist, S., and Rokeach, L. A. (2009) The *Schizosaccharomyces pombe* Hsp104 disaggregase is unable to propagate the [PSI] prion. *PLoS one* **4**, e6939
11. Coelho, M., Dereli, A., Haese, A., Kuhn, S., Malinowska, L., Desantis, M. E., Shorter, J., Alberti, S., Gross, T., and Tolic-Norrelykke, I. M. (2013) Fission Yeast Does Not Age under Favorable Conditions, but Does So after Stress. *Current biology : CB* **23**, 1844-1852
12. Parsell, D. A., Kowal, A. S., and Lindquist, S. (1994) *Saccharomyces cerevisiae* Hsp104 protein. Purification and characterization of ATP-induced structural changes. *J. Biol. Chem.* **269**, 4480-4487
13. Zolkiewski, M., Kessel, M., Ginsburg, A., and Maurizi, M. R. (1999) Nucleotide-dependent oligomerization of ClpB from *Escherichia coli*. *Prot. Sci.* **8**, 1899-1903
14. Lee, S., Sowa, M. E., Watanabe, Y. H., Sigler, P. B., Chiu, W., Yoshida, M., and Tsai, F. T. (2003) The structure of ClpB: a molecular chaperone that rescues proteins from an aggregated state. *Cell* **115**, 229-240
15. Mackay, R. G., Helsen, C. W., Tkach, J. M., and Glover, J. R. (2008) The C-terminal extension of *Saccharomyces cerevisiae* Hsp104 plays a role in oligomer assembly. *Biochemistry* **47**, 1918-1927

16. Doyle, S. M., and Wickner, S. (2009) Hsp104 and ClpB: protein disaggregating machines. *Trends Biochem Sci* **34**, 40-48
17. Haslberger, T., Bukau, B., and Mogk, A. (2010) Towards a unifying mechanism for ClpB/Hsp104-mediated protein disaggregation and prion propagation. *Biochem. Cell. Biol.* **88**, 63-75
18. Tipton, K. A., Verges, K. J., and Weissman, J. S. (2008) In vivo monitoring of the prion replication cycle reveals a critical role for Sis1 in delivering substrates to Hsp104. *Mol Cell* **32**, 584-591
19. Miot, M., Reidy, M., Doyle, S. M., Hoskins, J. R., Johnston, D. M., Genest, O., Vitery, M. C., Masison, D. C., and Wickner, S. (2011) Species-specific collaboration of heat shock proteins (Hsp) 70 and 100 in thermotolerance and protein disaggregation. *Proc Natl Acad Sci U S A* **108**, 6915-6920
20. Sielaff, B., and Tsai, F. T. (2010) The M-domain controls Hsp104 protein remodeling activity in an Hsp70/Hsp40-dependent manner. *J Mol Biol* **402**, 30-37
21. Haslberger, T., Zdanowicz, A., Brand, I., Kirstein, J., Turgay, K., Mogk, A., and Bukau, B. (2008) Protein disaggregation by the AAA+ chaperone ClpB involves partial threading of looped polypeptide segments. *Nat Struct Mol Biol* **15**, 641-650
22. Weibezahn, J., Tessarz, P., Schlieker, C., Zahn, R., Maglica, Z., Lee, S., Zentgraf, H., Weber-Ban, E. U., Dougan, D. A., Tsai, F. T., Mogk, A., and Bukau, B. (2004) Thermotolerance requires refolding of aggregated proteins by substrate translocation through the central pore of ClpB. *Cell* **119**, 653-665
23. Lum, R., Tkach, J. M., Vierling, E., and Glover, J. R. (2004) Evidence for an unfolding/threading mechanism for protein disaggregation by *Saccharomyces cerevisiae* Hsp104. *J. Biol. Chem.* **279**, 29139-29146
24. Tessarz, P., Mogk, A., and Bukau, B. (2008) Substrate threading through the central pore of the Hsp104 chaperone as a common mechanism for protein disaggregation and prion propagation. *Mol. Microbiol.* **68**, 87-97
25. Shorter, J., and Lindquist, S. (2005) Navigating the ClpB channel to solution. *Nat Struct Mol Biol* **12**, 4-6
26. DeSantis, M. E., Leung, E. H., Sweeny, E. A., Jackrel, M. E., Cushman-Nick, M., Neuhaus-Follini, A., Vashist, S., Sochor, M. A., Knight, M. N., and Shorter, J. (2012) Operational plasticity enables Hsp104 to disaggregate diverse amyloid and nonamyloid clients. *Cell* **151**, 778-793
27. Mogk, A., Schlieker, C., Strub, C., Rist, W., Weibezahn, J., and Bukau, B. (2003) Roles of individual domains and conserved motifs of the AAA+ chaperone ClpB in oligomerization, ATP hydrolysis, and chaperone activity. *J. Biol. Chem.* **278**, 17615-17624
28. Schirmer, E. C., Ware, D. M., Queitsch, C., Kowal, A. S., and Lindquist, S. L. (2001) Subunit interactions influence the biochemical and biological properties of Hsp104. *Proc. Natl. Acad. Sci. U.S.A.* **98**, 914-919
29. Schirmer, E. C., Queitsch, C., Kowal, A. S., Parsell, D. A., and Lindquist, S. (1998) The ATPase activity of Hsp104, effects of environmental conditions and mutations. *J. Biol. Chem.* **273**, 15546-15552
30. Hattendorf, D. A., and Lindquist, S. L. (2002) Cooperative kinetics of both Hsp104 ATPase domains and interdomain communication revealed by AAA sensor-1 mutants. *EMBO J.* **21**, 12-21
31. Hattendorf, D. A., and Lindquist, S. L. (2002) Analysis of the AAA sensor-2 motif in the C-terminal ATPase domain of Hsp104 with a site-specific fluorescent probe of nucleotide binding. *Proc. Natl. Acad. Sci. U.S.A.* **99**, 2732-2737
32. Doyle, S. M., Shorter, J., Zolkiewski, M., Hoskins, J. R., Lindquist, S., and Wickner, S. (2007) Asymmetric deceleration of ClpB or Hsp104 ATPase activity unleashes protein-remodeling activity. *Nat Struct Mol Biol* **14**, 114-122

33. Reidy, M., Miot, M., and Masison, D. C. (2012) Prokaryotic chaperones support yeast prions and thermotolerance and define disaggregation machinery interactions. *Genetics* **192**, 185-193
34. Lo Bianco, C., Shorter, J., Regulier, E., Lashuel, H., Iwatsubo, T., Lindquist, S., and Aebischer, P. (2008) Hsp104 antagonizes alpha-synuclein aggregation and reduces dopaminergic degeneration in a rat model of Parkinson disease. *J. Clin. Invest.* **118**, 3087-3097
35. Shorter, J., and Lindquist, S. (2004) Hsp104 catalyzes formation and elimination of self-replicating Sup35 prion conformers. *Science* **304**, 1793-1797
36. Hinault, M. P., Cuendet, A. F., Mattoo, R. U., Mensi, M., Dietler, G., Lashuel, H. A., and Goloubinoff, P. (2010) Stable alpha-synuclein oligomers strongly inhibit chaperone activity of the Hsp70 system by weak interactions with J-domain co-chaperones. *J. Biol. Chem.* **285**, 38173-38182
37. DeSantis, M. E., and Shorter, J. (2012) Hsp104 drives "protein-only" positive selection of Sup35 prion strains encoding strong [PSI(+)]. *Chemistry & biology* **19**, 1400-1410
38. Werbeck, N. D., Schlee, S., and Reinstein, J. (2008) Coupling and Dynamics of Subunits in the Hexameric AAA+ Chaperone ClpB. *J. Mol. Biol.* **378**, 178-190
39. Zhang, T., Kedzierska-Mieszkowska, S., Liu, H., Cheng, C., Ganta, R. R., and Zolkiewski, M. (2013) Aggregate-reactivation activity of the molecular chaperone ClpB from *Ehrlichia chaffeensis*. *PloS one* **8**, e62454
40. Zolkiewski, M. (1999) ClpB cooperates with DnaK, DnaJ, and GrpE in suppressing protein aggregation. A novel multi-chaperone system from *Escherichia coli*. *J. Biol. Chem.* **274**, 28083 - 28086
41. Doyle, S. M., Hoskins, J. R., and Wickner, S. (2007) Collaboration between the ClpB AAA+ remodeling protein and the DnaK chaperone system. *Proc Natl Acad Sci U S A* **104**, 11138-11144
42. Saibil, H. R. (2013) Biochemistry. Machinery to reverse irreversible aggregates. *Science* **339**, 1040-1041
43. Krzewska, J., Langer, T., and Liberek, K. (2001) Mitochondrial Hsp78, a member of the Clp/Hsp100 family in *Saccharomyces cerevisiae*, cooperates with Hsp70 in protein refolding. *FEBS Lett.* **489**, 92-96
44. Rosenzweig, R., Moradi, S., Zarrine-Afsar, A., Glover, J. R., and Kay, L. E. (2013) Unraveling the mechanism of protein disaggregation through a ClpB-DnaK interaction. *Science* **339**, 1080-1083
45. Seyffer, F., Kummer, E., Oguchi, Y., Winkler, J., Kumar, M., Zahn, R., Sourjik, V., Bukau, B., and Mogk, A. (2012) Hsp70 proteins bind Hsp100 regulatory M domains to activate AAA+ disaggregase at aggregate surfaces. *Nat Struct Mol Biol* **19**, 1347-1355
46. Lee, J., Kim, J. H., Biter, A. B., Sielaff, B., Lee, S., and Tsai, F. T. (2013) Heat shock protein (Hsp) 70 is an activator of the Hsp104 motor. *Proc. Natl. Acad. Sci. U.S.A.* **110**, 8513-8518
47. Haslberger, T., Weibezahn, J., Zahn, R., Lee, S., Tsai, F. T., Bukau, B., and Mogk, A. (2007) M domains couple the ClpB threading motor with the DnaK chaperone activity. *Mol Cell* **25**, 247-260
48. Oguchi, Y., Kummer, E., Seyffer, F., Berynsky, M., Anstett, B., Zahn, R., Wade, R. C., Mogk, A., and Bukau, B. (2012) A tightly regulated molecular toggle controls AAA+ disaggregase. *Nat Struct Mol Biol* **19**, 1338-1346
49. Lee, S., Sielaff, B., Lee, J., and Tsai, F. T. (2010) CryoEM structure of Hsp104 and its mechanistic implication for protein disaggregation. *Proc Natl Acad Sci U S A* **107**, 8135-8140
50. Wendler, P., and Saibil, H. R. (2010) Cryo electron microscopy structures of Hsp100 proteins: crowbars in or out? *Biochem. Cell. Biol.* **88**, 89-96
51. Wendler, P., Shorter, J., Plisson, C., Cashikar, A. G., Lindquist, S., and Saibil, H. R. (2007) Atypical AAA+ Subunit Packing Creates an Expanded Cavity for Disaggregation by the Protein-Remodeling Factor Hsp104. *Cell* **131**, 1366-1377
52. Wendler, P., Shorter, J., Snead, D., Plisson, C., Clare, D. K., Lindquist, S., and Saibil, H. R. (2009) Motor Mechanism for Protein Threading through Hsp104. *Mol. Cell* **34**, 81-92

53. Lee, S., Choi, J. M., and Tsai, F. T. (2007) Visualizing the ATPase cycle in a protein disaggregating machine: structural basis for substrate binding by ClpB. *Mol Cell* **25**, 261-271
54. Sweeny, E. A., DeSantis, M. E., and Shorter, J. (2011) Purification of Hsp104, a protein disaggregase. *J. Vis. Exp.* **55**, e3190
55. Sun, Z., Diaz, Z., Fang, X., Hart, M. P., Chesi, A., Shorter, J., and Gitler, A. D. (2011) Molecular determinants and genetic modifiers of aggregation and toxicity for the ALS disease protein FUS/TLS. *PLoS Biol.* **9**, e1000614
56. Gupta, S., Sullivan, M., Toomey, J., Kiselar, J., and Chance, M. R. (2007) The Beamline X28C of the Center for Synchrotron Biosciences: a national resource for biomolecular structure and dynamics experiments using synchrotron footprinting. *Journal of synchrotron radiation* **14**, 233-243
57. Mayne, L., Kan, Z. Y., Chetty, P. S., Ricciuti, A., Walters, B. T., and Englander, S. W. (2011) Many overlapping peptides for protein hydrogen exchange experiments by the fragment separation-mass spectrometry method. *J Am Soc Mass Spectrom* **22**, 1898-1905
58. Kaur, P., Kiselar, J. G., and Chance, M. R. (2009) Integrated algorithms for high-throughput examination of covalently labeled biomolecules by structural mass spectrometry. *Anal. Chem.* **81**, 8141-8149
59. Konarev, P. V., Volkov, V. V., Sokolova, A. V., Koch, M. H. J., and Svergun, D. I. (2003) PRIMUS: a Windows PC-based system for small-angle scattering data analysis. *J. Appl. Cryst.* **36**, 1277-1282
60. Rice, S. A. (1956) Small angle scattering of X-rays. A. Guinier and G. Fournet. Translated by C. B. Wilson and with a bibliographical appendix by K. L. Yudowitch. Wiley, New York, 1955. *Journal of Polymer Science* **19**, 594-594
61. Svergun, D. (1992) Determination of the regularization parameter in indirect-transform methods using perceptual criteria. *J. Appl. Cryst.* **25**, 495-503
62. Wang, F., Mei, Z., Qi, Y., Yan, C., Hu, Q., Wang, J., and Shi, Y. (2011) Structure and mechanism of the hexameric MecA-ClpC molecular machine. *Nature* **471**, 331-335
63. Cashikar, A. G., Schirmer, E. C., Hattendorf, D. A., Glover, J. R., Ramakrishnan, M. S., Ware, D. M., and Lindquist, S. L. (2002) Defining a pathway of communication from the C-terminal peptide binding domain to the N-terminal ATPase domain in a AAA protein. *Mol Cell* **9**, 751-760
64. Lakowicz, J. R. (1983) *Principles of Fluorescence Spectroscopy*, Plenum Press, New York, NY
65. Eftink, M. R., and Ghiron, C. A. (1981) Fluorescence quenching studies with proteins. *Anal. Biochem.* **114**, 199-227
66. Xu, G., Kiselar, J., He, Q., and Chance, M. R. (2005) Secondary Reactions and Strategies To Improve Quantitative Protein Footprinting. *Anal. Chem.* **77**, 3029-3037
67. Xu, G., and Chance, M. R. (2007) Hydroxyl Radical-Mediated Modification of Proteins as Probes for Structural Proteomics. *Chem. Rev.* **107**, 3514-3543
68. Takamoto, K., and Chance, M. R. (2006) Radiolytic protein footprinting with mass spectrometry to probe the structure of macromolecular complexes. *Annu. Rev. Biophys. Biomol. Struct.* **35**, 251-276
69. Bohon, J., Jennings, L. D., Phillips, C. M., Licht, S., and Chance, M. R. (2008) Synchrotron protein footprinting supports substrate translocation by ClpA via ATP-induced movements of the D2 loop. *Structure* **16**, 1157-1165
70. Rambo, R. P., and Tainer, J. A. (2011) Characterizing flexible and intrinsically unstructured biological macromolecules by SAS using the Porod-Debye law. *Biopolymers* **95**, 559-571
71. Rambo, R. P., and Tainer, J. A. (2013) Accurate assessment of mass, models and resolution by small-angle scattering. *Nature* **496**, 477-481

Acknowledgments

We thank Laura Castellano, Meredith Jackrel, Lin Guo, Mariana Torrente (University of Pennsylvania), and Helen Saibil (Birkbeck College) for helpful suggestions; Sue Lindquist (Whitehead Institute, MIT) for generous provision of reagents; Greg Van Duyne, Jane Vanderkooi, Zhongyuan Kan, Matthew

Sochor, and Walter Englander (University of Pennsylvania) for assistance with SAXS, Trp fluorescence, and XF experiments; Beamline X9 at NSLS for SAXS/WAXS collection and beamline X28C at NSLS for XF data collection. Our work was funded by NIH training grant (T32GM071339) and NRSA predoctoral fellowship (F31NS079009) (M.E.D.); NIH training grant (T32GM008275) and American Heart Association predoctoral fellowship (E.A.S.); NIH Director's New Innovator Award (DP2OD002177), Ellison Medical Foundation New Scholar in Aging Award, and NIH grant R01GM099836 (J.S.).

Figure legends

Figure 1. Location of the MD distal loop. (A) Domain schematic of Hsp104. N-terminal domain is shown in brown, NBD1 in yellow, MD in purple, NBD2 in blue, and the C-terminal extension in green. (B) Homology model of the Hsp104 monomer with the conserved distal loop residues A430 (orange), L431 (teal), and D438 (blue) are shown as spheres. Domain coloring is as in (A). (C) Homology model of the Hsp104 MD. Helix 1 is shown in purple, helix 2 in blue, helix 3 in yellow, and helix 4 in green. MD residues studied in this paper are indicated as spheres: A430 (orange), L431 (teal), A437 (pink), D438 (blue), A453 (dark green), Y466 (light green), Y497 (dark orange), and Y507 (grey). (D) ClustalW alignment of the middle domains from several Hsp104 homologues. The MD is shaded blue. Helix 1 is boxed in purple, the distal loop region is boxed in red, helix 2 is boxed in blue, helix 3 is boxed in yellow, and helix 4 is boxed in green. Arrows indicate A430, L431, A437, and D438.

Figure 2. Hsp104^{Y507A} is a hypomorph with altered intrinsic disaggregase activity. (A) $\Delta hsp104$ yeast cells harboring empty pHSE vector (black markers), pHSE-Hsp104 (blue markers), or pHSE-Hsp104^{Y507A} (red markers) were grown to mid-log phase in SD-ura liquid. Prior to the 50°C heat treatment, matched cultures were preincubated at 37°C for 30min. Following treatment at 50°C for 0–20min cells were transferred to ice, diluted in ice-cold SD-ura, immediately plated on SD-ura, and allowed to recover for 3 days at 30°C and cell viability was assessed. Values represent means±SEM (n=4). A one-way ANOVA with the post-hoc Dunnett's multiple comparisons test was used to compare vector alone to the Hsp104^{WT} and Hsp104^{Y507A} constructs (* denotes p<0.05). (B) $\Delta hsp104$ yeast cells harboring pGPD-LuxAB (encoding a temperature sensitive luciferase fusion protein) and either empty vector (pHSE), pHSE-Hsp104, or pHSE-Hsp104^{Y507A} were grown to mid-log phase in SD-his-ura liquid. Matched cultures were preincubated at 37°C for 30 min and then incubated at 44°C for 50 min. Cycloheximide (10µg/ml) was then added and cultures were incubated for a further 10 min at 44°C. Cells were then shifted to 30°C and luciferase activity was measured at 0, 90, and 120min. Luciferase activity was expressed as the % of WT Hsp104 condition after 120min. Values represent means±SEM (n=3). (C) Urea-denatured firefly luciferase aggregates were incubated for 90min at 25°C with Hsp104 (1µM) or Hsp104^{Y507A} (1µM) in the presence of ATP (5.1mM), a mixture of ATP (1mM) and ATPγS (4mM), or Hsc70 (an Hsp70) (1µM) and Hdj2 (an Hsp40) (1µM) plus ATP (5.1mM). Reactivation of luciferase was then determined by luminescence and converted to % WT disassembly activity (activity of 1µM WT Hsp104 in the presence of Hsc70 and Hdj2). Values represent means±SEM (n=3). (D) Urea-denatured firefly luciferase aggregates were incubated for 60min at 25°C with ClpB (0.167µM) or ClpB^{Y503A} (0.167µM) in the presence of either ATP (5.1mM), a mixture of ATP (2.5mM) and ATPγS (2.5mM), or DnaK (1µM), DnaJ (0.033µM), and GrpE (0.0167µM) plus ATP (5.1mM). Reactivation of luciferase was then determined by luminescence and converted to % WT ClpB activity (activity of 0.167µM WT ClpB in the presence of DnaK, DnaJ, and GrpE). Values represent means±SEM (n=3).

Figure 3. Hsp104^{A430W}, Hsp104^{L431W}, and Hsp104^{D438W} are specifically defective in Hsp70 collaboration. (A) Urea-denatured firefly luciferase aggregates were incubated for 90min at 25°C with Hsp104 (1µM) or the indicated Hsp104 variant (1µM) plus ATP (1mM) and ATPγS (4mM). Luciferase reactivation was then determined and converted to % WT disaggregase activity in the presence of ATPγS:ATP. Values represent means±SEM (n=3-10). A one-way ANOVA with the post-hoc Dunnett's

multiple comparisons test was used to compare Hsp104^{WT} to Hsp104 variants (* denotes p<0.05). **(B)** Reactions were performed as in **(A)** except that the mixture of ATP (1mM) and ATP γ S (4mM) was replaced with ATP (5.1mM). Values represent means \pm SEM (n=3-13). A one-way ANOVA with the post-hoc Dunnett's multiple comparisons test was used to compare Hsp104^{WT} to Hsp104 variants (* denotes p<0.05). **(C)** Reactions were performed as in **(A)** except that ATP (1mM) and ATP γ S (4mM) was replaced with Hsc70 (1 μ M) and Hdj2 (1 μ M) plus ATP (5.1mM). Luciferase reactivation was then determined and converted to % WT disaggregase activity in the presence of the Hsc70 and Hdj2. Values represent means \pm SEM (n=3-10). A one-way ANOVA with the post-hoc Dunnett's multiple comparisons test was used to compare Hsp104^{WT} to Hsp104 variants (* denotes p<0.05). **(D)** Δ *hsp104* yeast cells harboring empty pHSE vector (black markers) or the indicated pHSE-Hsp104 variant (WT, A430W, A437W, A453W, Y466W, Y497W, or Y507W) were grown to mid-log phase in SD-ura liquid. Prior to the 50°C heat treatment, matched cultures were preincubated at 37°C for 30min. Following treatment at 50°C for 0–20 min cells were transferred to ice, diluted in ice-cold SD-ura, immediately plated on SD-ura, and allowed to recover for 3 days at 30°C and cell viability was assessed. Note that all the Hsp104 variants retain WT levels except of activity except Hsp104^{A430W}, which behaves as a null allele. Values represent means \pm SEM (n=3). We employed a one-way ANOVA with the post-hoc Dunnett's multiple comparisons test was used to compare vector alone to each Hsp104 variant (* denotes p<0.05). **(E)** Δ *hsp104* yeast cells harboring empty pHSE vector (black markers) or the indicated pHSE-Hsp104 variant (WT, A430W, L431W, or D438W) were grown to mid-log phase in SD-ura liquid. Prior to the 50°C heat treatment, matched cultures were preincubated at 37°C for 30min. Following treatment at 50°C for 0–20min cells were transferred to ice, and spotted in five-fold serial dilutions on SD-ura. Cells were allowed to recover for 3 days at 30°C and cell viability was assessed. **(F)** Urea-denatured firefly luciferase aggregates were incubated for 60min at 25°C with ClpB (0.167 μ M) or ClpB^{A428W} plus ATP (2.5mM) and ATP γ S (2.5mM). Luciferase reactivation was then determined and converted to % WT disaggregase activity in the presence of ATP γ S:ATP. Values represent means \pm SEM (n=4). A t-test was used to compare ClpB to ClpB^{A428W} (* denotes p<0.05). **(G)** Reactions were performed as in **(F)** except that the mixture of ATP and ATP γ S was replaced with ATP (5.1mM). Values represent means \pm SEM (n=3). A t-test was used to compare ClpB to ClpB^{A428W} (* denotes p<0.05). **(H)** Reactions were performed as in **(F)** except that the mixture of ATP and ATP γ S was replaced with DnaK (1 μ M), DnaJ (0.033 μ M), and GrpE (0.0167 μ M) plus ATP (5.1mM). Reactivation of luciferase was then determined by luminescence and converted to % WT disaggregase activity in the presence of the Hsp70 chaperone system. Values represent means \pm SEM (n=4). A t-test was used to compare ClpB to ClpB^{A428W} (* denotes p<0.05).

Figure 4. Reduced ATPase activity does not explain inability of specific distal loop variants to collaborate with Hsp70. **(A)** The indicated Hsp104 or ClpB variants (0.25 μ M) were incubated for 12min (Hsp104 variants) or 30min (ClpB variants) with ATP (1mM) and resulting ATPase rates were determined. Values represent means \pm SEM (n=3-9). A one-way ANOVA with the post-hoc Dunnett's multiple comparisons test was used to compare Hsp104^{WT} to Hsp104 variants. A t-test was used to compare ClpB to ClpB^{A428W} (* denotes p<0.05). **(B)** Reactivation of luciferase in the presence of Hsc70, and Hdj2 is plotted against ATPase activity for WT Hsp104 and variants. Positions of WT, A430W, A430V, L431D, and D438A are indicated. Values represent means \pm SEM (n=3-9). A simple linear regression yielded a coefficient of determination, R²=0.1994. **(C)** Reactivation of luciferase in the presence of ATP γ S:ATP is plotted against ATPase activity for WT Hsp104 and variants. Positions of WT, A430W, A430V, L431D, and D438A are indicated. Values represent means \pm SEM (n=3-10). A simple linear regression yielded a coefficient of determination, R²=0.012.

Figure 5. The distal loop of the Hsp104 MD is partially solvent inaccessible. **(A-D)** Tryptophan fluorescence spectra of Hsp104^{Y466W} (green line), Hsp104^{Y497W} (purple line), Hsp104^{A430W} (orange line), Hsp104^{L431W} (light blue line), Hsp104^{A437W} (red line) or Hsp104^{D438W} (dark blue line). All variants were left in the apo state **(A)** or incubated with ATP **(B)**, ATP γ S **(C)**, or ADP **(D)** for 15min prior to measurements. Samples were excited at 295nm (4nm bandwidth) and emission was collected from 305-

505nm (3nm bandwidth). Each spectrum is an average of two readings. **(E)** Dose-response curves for Hsp104 peptide 431-455 showing fraction unmodified as a function of x-ray exposure time in the presence of ATP γ S (blue triangles) or ADP (black squares). The distal loop residues are highlighted in red. Values represent means \pm SEM (n=3-4). **(F, G)** Comparison of published **(F)** (52) and an optimized **(G)** rigid body domain fit of Hsp104 homology model into the cryo-EM map of Hsp104^{N728A} in the presence of ATP. Only one subunit is depicted. Domains are color coded as follows: NDB1, orange; MD, purple; NBD2, teal. The resolution of the map does not allow for an unambiguous fit of the MD domain relative to NBD1 and NBD2. Possible fits are distinguished by a rotation of the MD around helix 2, which swaps the NBD2 contacts at the distal end of the MD. Cross-linking experiments confirmed the optimized fit **(G)** to be more accurate (see Fig. 6 and 7).

Figure 6. The distal loop of the MD can contact NBD2 in Hsp104 and ClpB. **(A)** Successful disulfide crosslinks formed between the MD (pink) and NBD2 (blue) of Hsp104 (only one monomer shown) as predicted by the optimized Hsp104 rigid body fit of the Hsp104^{N728A} hexamer in the presence of ATP (Fig. 5G) (52). Residue A430C (dark purple spheres) in the MD could crosslink to F630C (light purple spheres) in NBD2. Residue K451C (dark green spheres) in the MD could crosslink to E790C (light green spheres) in NBD2. **(B, C)** Intramolecular disulfide crosslinks formed between A430C and F630C **(B)** and K451C and E790C **(C)** in the presence of ADP, ATP, or AMP-PNP. Reduced and oxidized Hsp104 variants (+/- DTT) were analyzed by non-reducing SDS-PAGE. Crosslinks were visualized by band up-shift in SDS-PAGE (arrowheads indicated up-shifted species). Single cysteine mutant controls did not show crosslinking. Up-shift was seen only in double cysteine mutants. **(D)** The extent of disulfide formation monitored as in **(B, C)** was quantified using Ellman's reagent. Values represent means \pm SEM (n=3). **(E)** Successful disulfide crosslinks formed between the MD (pink) and NBD2 (blue) of ClpB (only one monomer shown) as deduced from the optimized Hsp104 rigid body fit of the Hsp104^{N728A} hexamer in the presence of ATP (52). Residue A428C (yellow spheres) in the MD could crosslink to L817C (orange spheres) in NBD2. **(F)** Intramolecular disulfide crosslinks formed between A428C and L817C in the presence of ADP, ATP, ATP γ S, or AMP-PNP. Reduced and oxidized ClpB variants (+/- DTT) were analyzed by non-reducing SDS-PAGE. Crosslinks were visualized by band up-shift in SDS-PAGE. Single cysteine mutant controls did not show crosslinking. Up-shift was seen only in double cysteine mutants (arrowhead indicates up-shifted species).

Figure 7. Defining NBD1-MD contacts in Hsp104. **(A, B)** Location of crosslinking pairs in the tClpB crystal structure **(A)** (14) compared to the homologous residues in the optimized Hsp104 rigid body fit of the Hsp104^{N728A} hexamer in the presence of ATP **(B)** (Fig. 5G) (52). Color-coded crosslinking pairs are listed in the insets and shown as sticks in the structures. The N-terminal domains are not shown for clarity. The MD is colored purple, NBD1 is colored yellow, and NBD2 is colored blue. **(C)** Disulfide crosslink formation of the indicated Hsp104^{C6S} variant was quantified using Ellman's reagent. Values represent means \pm SEM (n=2). **(D-J)** Reduced and oxidized Hsp104 variants (+/- DTT) were analyzed by non-reducing SDS-PAGE. Intramolecular disulfide crosslinks were visualized by band up-shift in SDS-PAGE. Single cysteine mutant controls did not show crosslinking **(D-J)**. Up-shift was seen only in specific double cysteine mutants: R336C:V540C **(D)**, K182C:E485C **(G)**, D247C:H471C **(H)**, D247C:E475C **(I)**, and E320C:N467C **(J)**. Two double cysteine mutants did not show any up-shift: I361C:K480C **(E)** and H362C:D484C **(F)**.

Figure 8. Crosslinking NBD2 to the distal loop diminishes disaggregase activity of Hsp104 and ClpB. **(A)** Urea-denatured firefly luciferase aggregates were incubated for 90min at 25°C with Hsp104 (1 μ M), Hsp104^{C6S} (1 μ M), or Hsp104^{6CS:A430C:F630C} in the presence of ATP (5.1mM), Hsc70 (1 μ M) and Hdj2 (1 μ M). Hsp104 variants were either not crosslinked (red), disulfide crosslinked with no DTT (blue), disulfide crosslinked and subsequently reduced with DTT (grey), or BMB crosslinked (green). The effect of BMB crosslinking on WT Hsp104 was not determined (denoted by ND). Reactivation of luciferase was then determined by luminescence and converted to % WT disassembly activity (activity of 1 μ M WT Hsp104 in the presence of Hsc70 and Hdj2). Values represent means \pm SEM (n=3). A one-way ANOVA

was performed to compare the means from each condition for each Hsp104 protein. The post-hoc Dunnett's multiple comparisons test was used to compare the not crosslinked control to the disulfide-linked, disulfide-linked+DTT, and BMB crosslinked conditions. * denotes $p < 0.05$. **(B)** Urea-denatured firefly luciferase aggregates were incubated for 90min at 25°C with ClpB (0.167 μ M), or ClpB^{A428C:L817C} (0.167 μ M) in the presence of ATP (5.1mM), DnaK (1 μ M), DnaJ (0.033 μ M), and GrpE (0.0167 μ M). ClpB variants were not crosslinked (red), disulfide crosslinked with no DTT (blue), or disulfide crosslinked and subsequently reduced with DTT (grey). Reactivation of luciferase was then determined by luminescence and converted to % WT disassembly activity (activity of 1 μ M WT ClpB in the presence of DnaK, DnaJ, and GrpE). Values represent means \pm SEM (n=3). A one-way ANOVA was performed to compare the means from each condition for each ClpB protein. The post-hoc Dunnett's multiple comparisons test was used to compare the not crosslinked control to the disulfide-linked, disulfide-linked+DTT, and BMB crosslinked conditions. * denotes $p < 0.05$. **(C)** ATPase activity of Hsp104^{6CS:A430C:F630C} after no crosslinking (red), disulfide crosslinking (blue), disulfide crosslinking followed by reduction with DTT (grey), or BMB crosslinking (green). Values represent means \pm SEM (n=3). A one-way ANOVA was performed to compare the means from each condition. The post-hoc Dunnett's multiple comparisons test was used to compare the not crosslinked control to the disulfide-linked, disulfide-linked+DTT, and BMB crosslinked conditions. * denotes $p < 0.05$. **(D)** ATPase activity of ClpB^{A428C:L817C} after no crosslinking (red), disulfide crosslinking (blue), or disulfide crosslinking followed by reduction with DTT (grey). Values represent means \pm SEM (n=3). A one-way ANOVA was performed to compare the means from each condition. The post-hoc Dunnett's multiple comparisons test was used to compare the not crosslinked control to the disulfide-linked, and disulfide-linked+DTT. No significant differences were found. **(E)** The A430W mutation in the distal loop changes the shape and compacts the Hsp104 hexamer. The P(r) distribution for WT Hsp104 (black line) and Hsp104^{A430W} (orange line) in the presence of ATP derived from SAXS data. The P(r) curves have been normalized to the area under the curve. The D_{max} and R_g values are summarized below (see Experimental Procedures and Table 1).

Figure 9. For disordered aggregate dissolution, Hsp104 hexamers require fewer subunits able to collaborate with Hsp70 than ClpB. **(A)** Theoretical ensembles of Hsp104 hexamers containing no mutant (black), one mutant subunit (blue), two (green), three (orange), four (red), five (purple) and six mutant subunits (yellow) as a function of the percentage of mutant subunits present. See Experimental Procedures for more details. **(B)** Theoretical activity curves for mutant doping experiments. The activity varies as a function of the percentage of mutant subunits present assuming that hexamer activity is proportional to the number of active subunits and all subunits in a hexamer are inactive when a specified number of mutant subunits per hexamer is breached. Curves are shown for situations where one or more mutant subunits (blue), two or more mutant subunits (red), three or more mutant subunits (green), four or more mutant subunits (purple), five or more mutant subunits (light blue), or six mutant subunits (orange) are required to eliminate hexamer activity. See Experimental Procedures for more details. **(C)** Urea-denatured luciferase aggregates were treated with Hsp104, Hsc70, and Hdj2 plus increasing fractions of, Hsp104^{A430W} (green markers). Alternatively, luciferase aggregates were treated with ClpB, ClpB^{A428W}, DnaK, and DnaJ. GrpE was included (grey markers) or omitted (orange markers). Where error bars are not visible, they are too small and are hidden by marker. Luciferase reactivation (% WT activity) was then assessed. Values represent means \pm SEM (n=3-4). Solid lines represent theoretical activity curves for situations where one or more mutant subunits (blue), two or more mutant subunits (red), three or more mutant subunits (green), four or more mutant subunits (purple), or five or more mutant subunits (light blue) are required to eliminate hexamer activity.

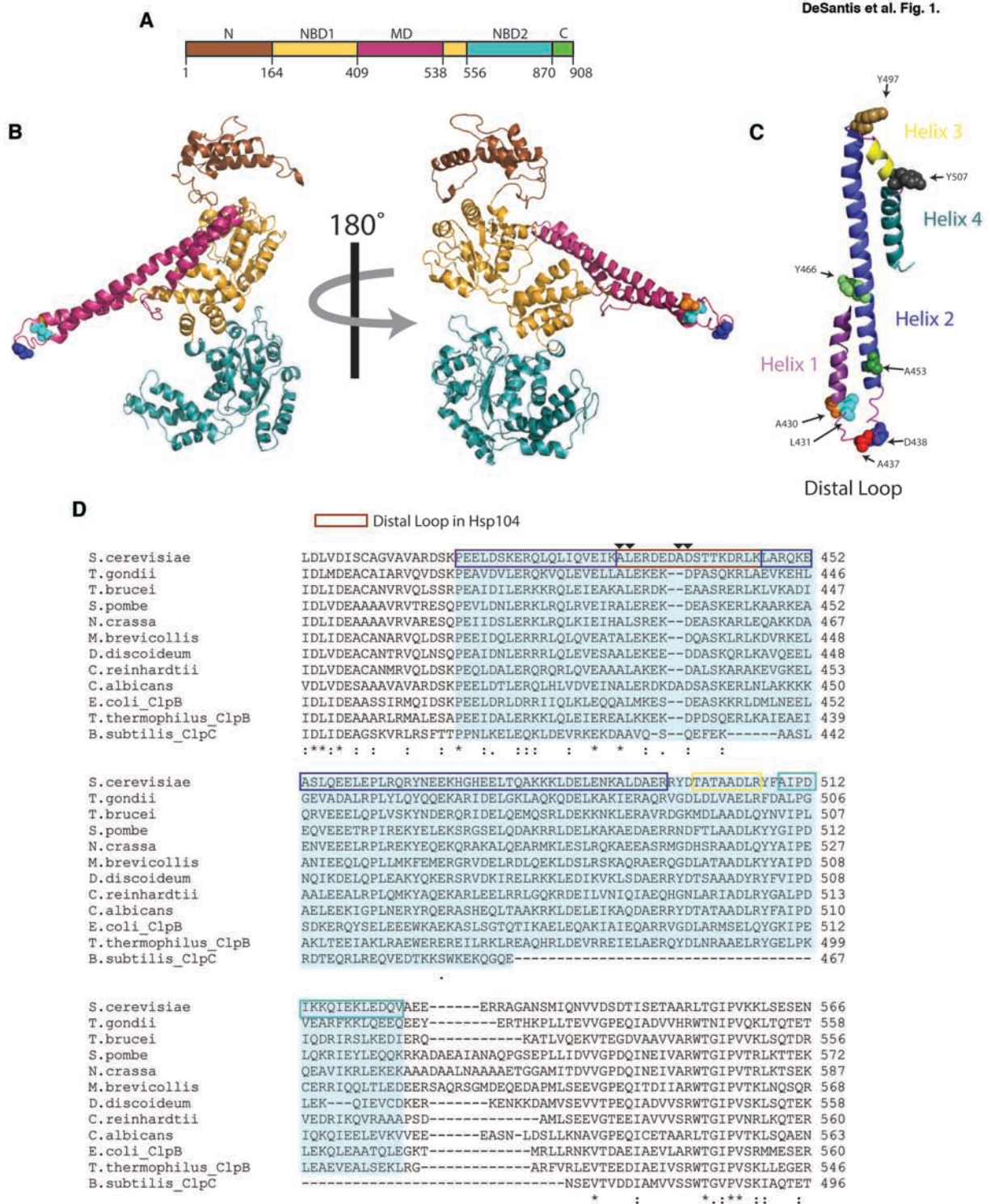
Table 1. Parameters Derived from SAXS for WT Hsp104 and Hsp104^{A430W} in the presence of ATP.

WT ATP		Guinier				GNOM				Porod		MM by Qr	
Location	Concentration	qmin	qRg range	Rg	I(0)	Angle range	Dmax	Rg	I(0)	Volume	P	Exp MM	Theor MM
NSLS	2.5 mg/mL	0.01	0.68-1.49	67.7+/-0.07	450.12 +/- 0.46	0.01-0.83	220	67.1	445	1654371	3.9	631000	612000
NSLS	5.0 mg/mL	0.01	0.75-1.50	68.1+/-0.05	936.03 +/- 0.69	0.01-0.81	230	68.2	935	1674270	3.9	645000	612000

A430W ATP		Guinier				GNOM				Porod		MM by Qr	
Location	Concentration	qmin	qRg range	Rg	I(0)	Angle range	Dmax	Rg	I(0)	Volume	P	Guinier	Theor MM
NSLS	1.5mg/mL	0.01	0.77-1.53	63.8+/-0.09	173.85+/-0.26	0.01-0.30	200	63.1	173	1569217	3.6	596000	612000
NSLS	2.1mg/mL	0.01	0.59-1.50	65.1+/-0.07	403.11 +/- 0.45	0.01-0.79	205	64	398	1595613	3.7	589000	612000

An R_g from the Guinier region of the scattering curve was determined using the program PRIMUS (59). Distance distribution functions $P(r)$ were calculated by the program GNOM using an indirect Fourier transform (61). The maximum dimension of the particle (D_{max}) was determined by examining the quality of fit to the experimental data for a D_{max} range of 180Å to 280Å, varied in 5Å increments. Values for R_g were computed from the second moment of the $P(r)$. The Porod volume and P value were calculated by the java-based program ScÅtter: <http://www.bioisis.net/tutorial/9>. The mass of the particle was calculated from Qr as described (71). See also Experimental Procedures.

Figure 1



Downloaded from <http://www.jbc.org/> at University of Pennsylvania Library on November 26, 2013

Figure 2

Fig. 2. DeSantis et al.

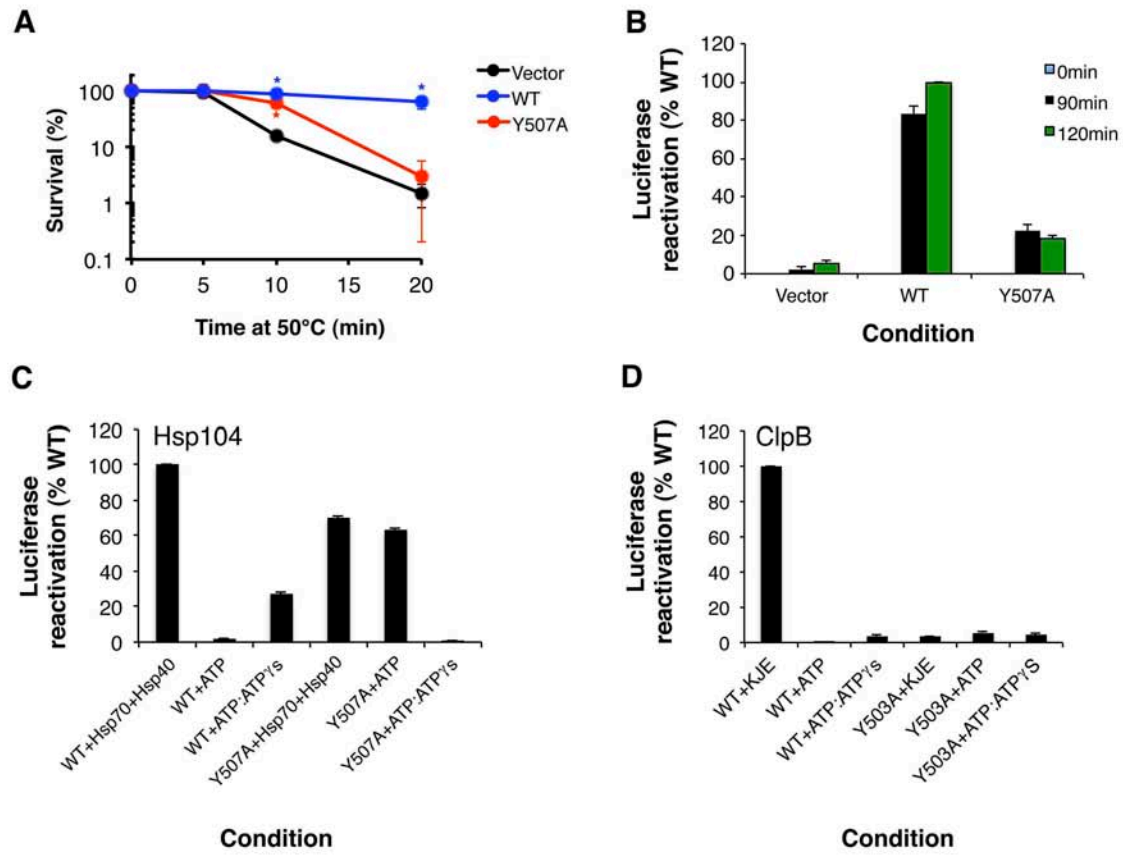


Figure 3

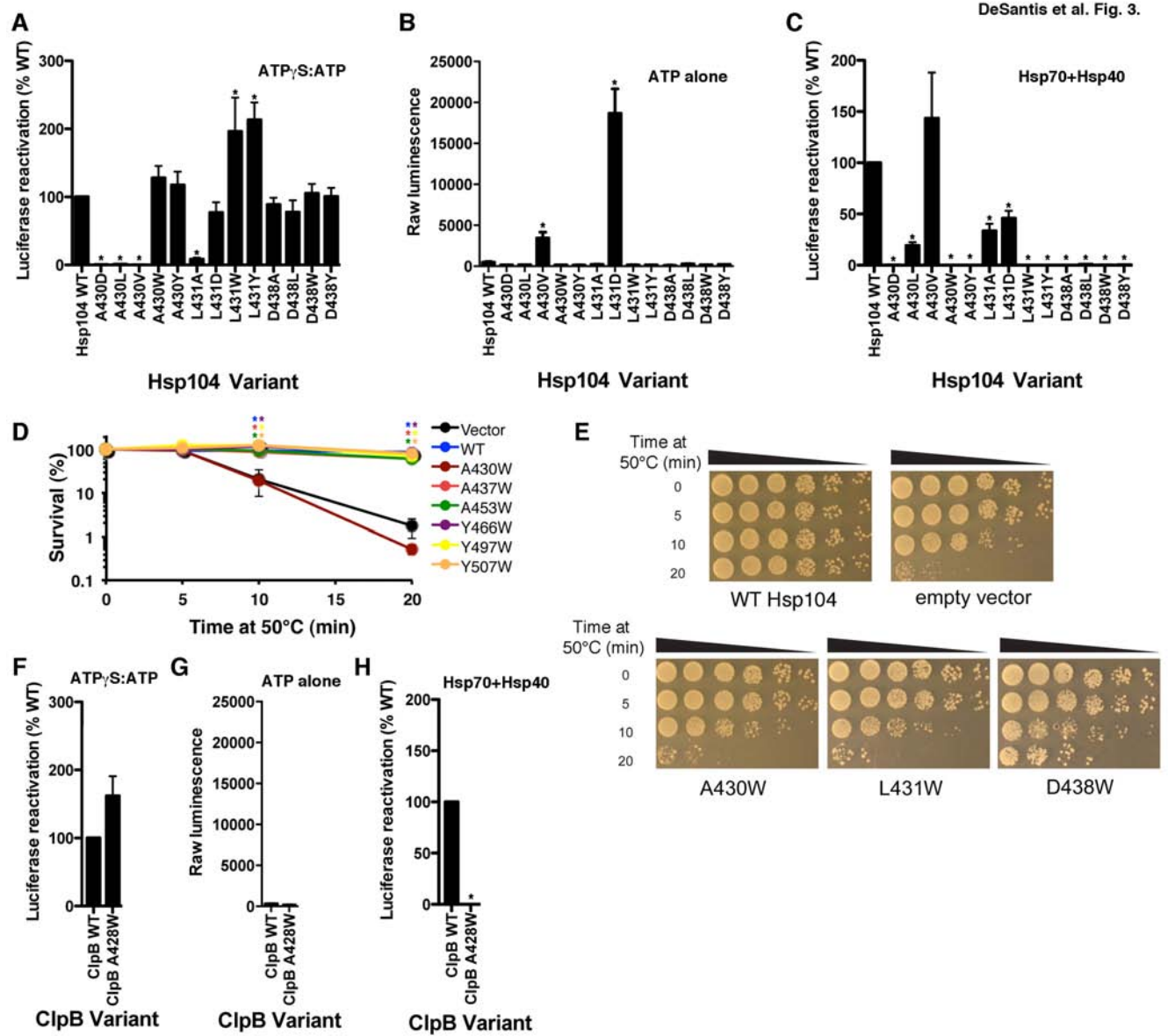


Figure 4

Fig. 4. DeSantis et al.

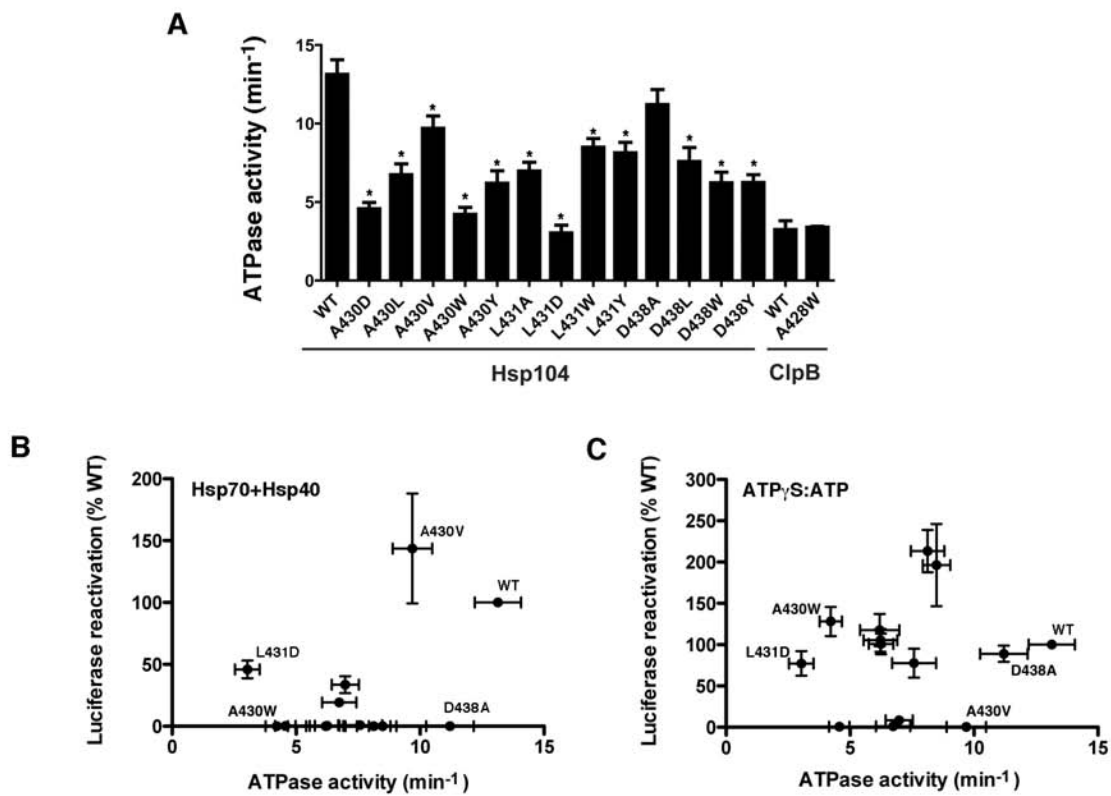


Figure 5

Fig. 5. DeSantis et al.

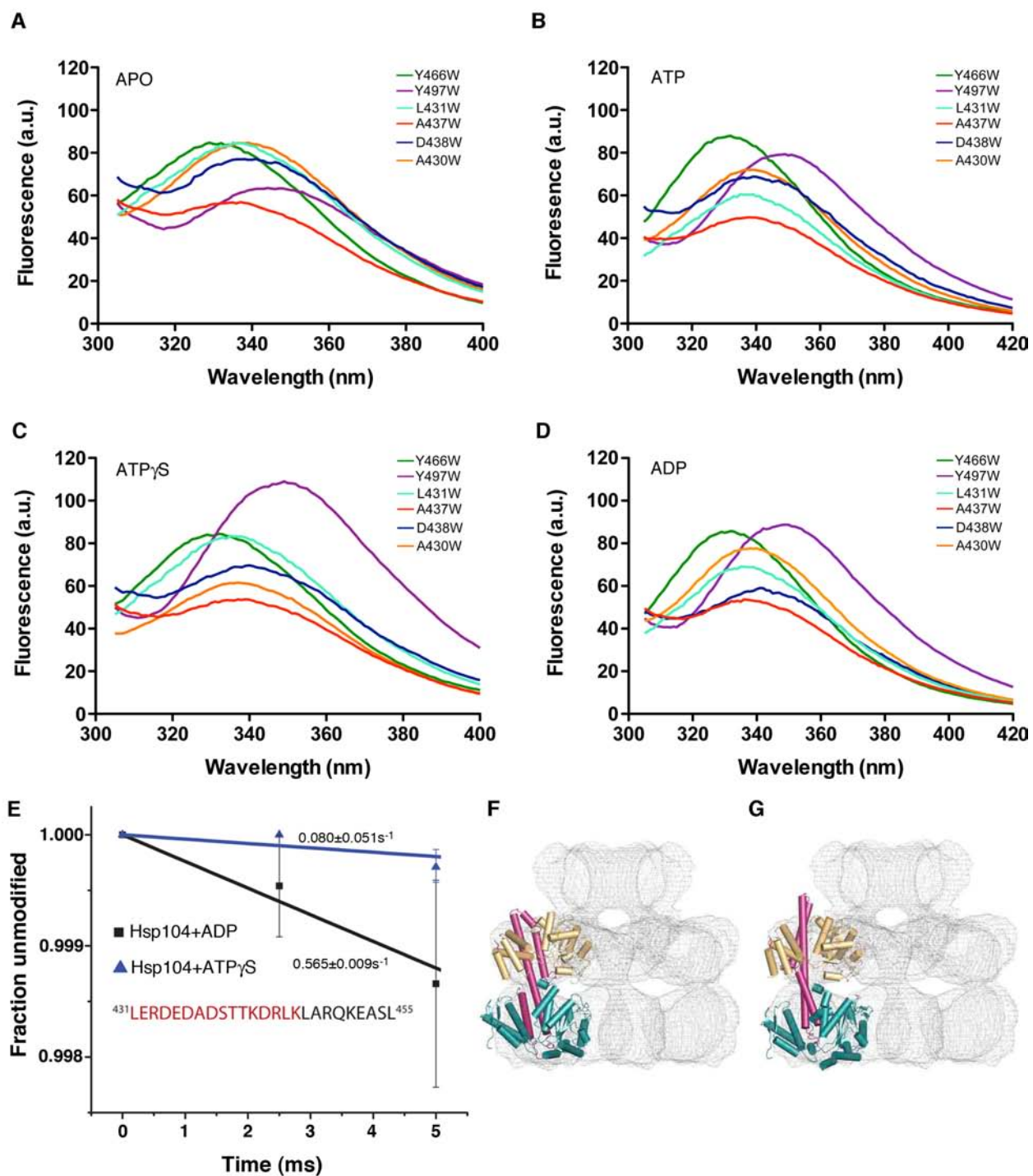


Figure 6

Fig. 6. DeSantis et al.

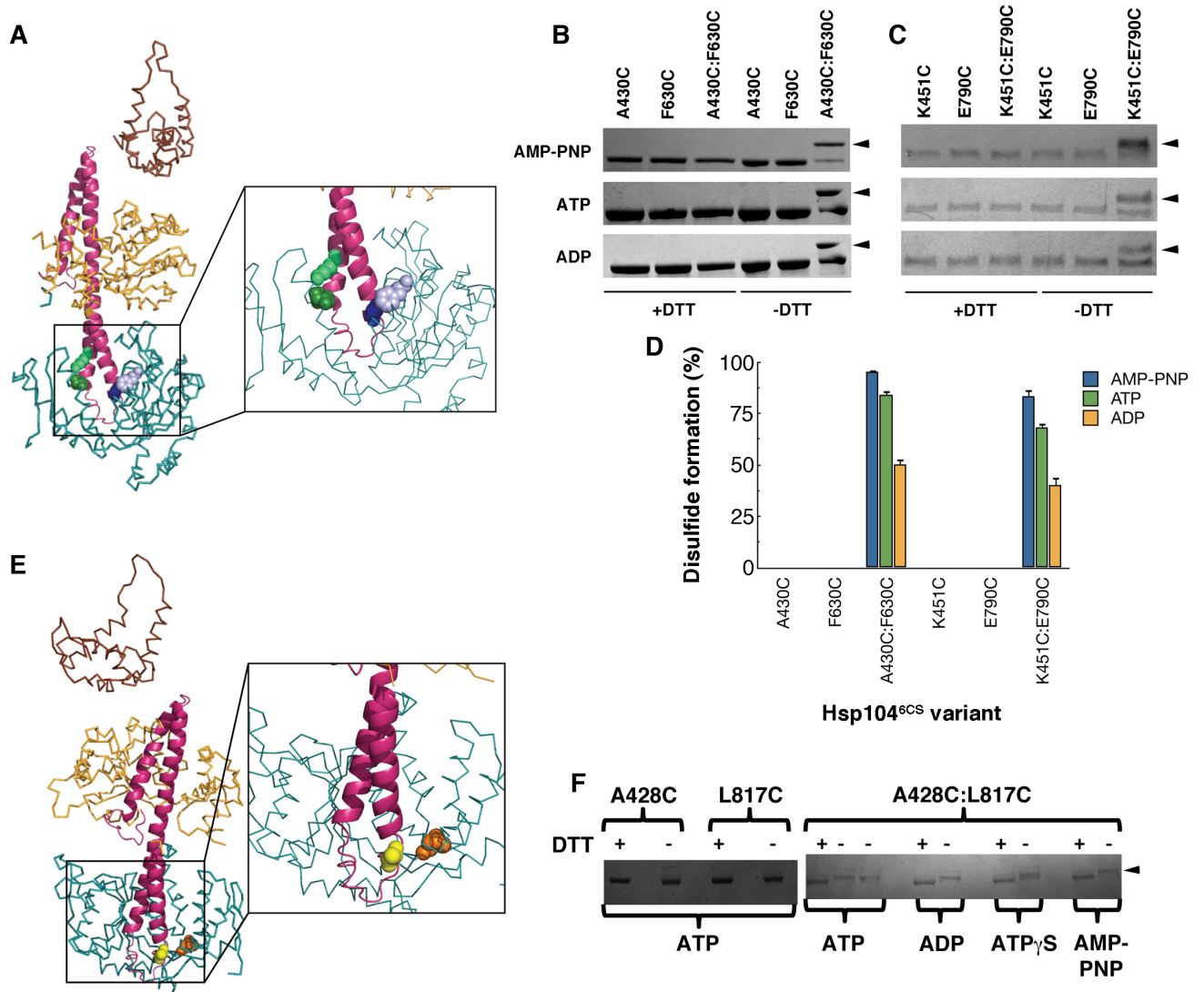


Figure 7

Fig. 7. DeSantis et al.

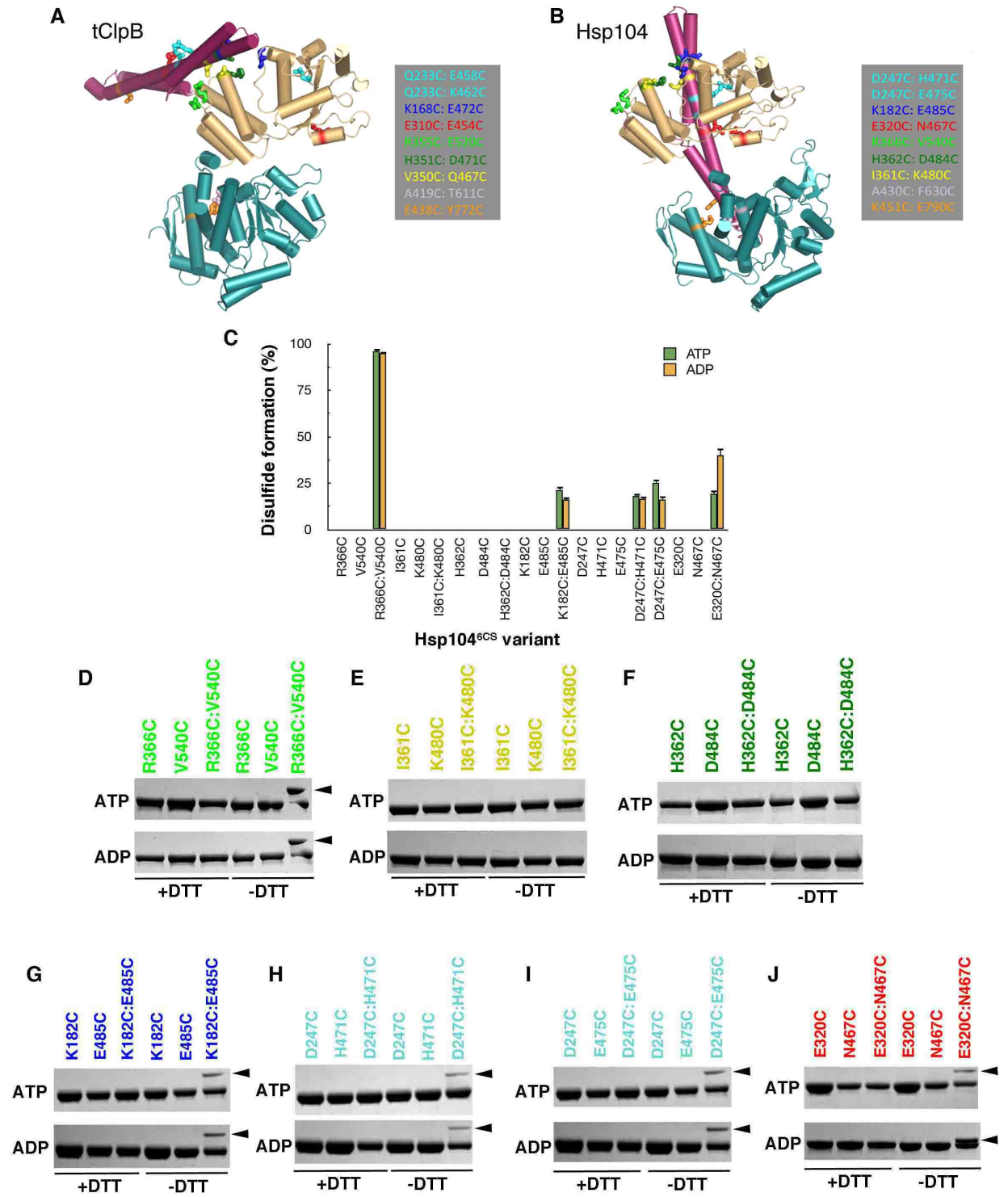


Figure 8

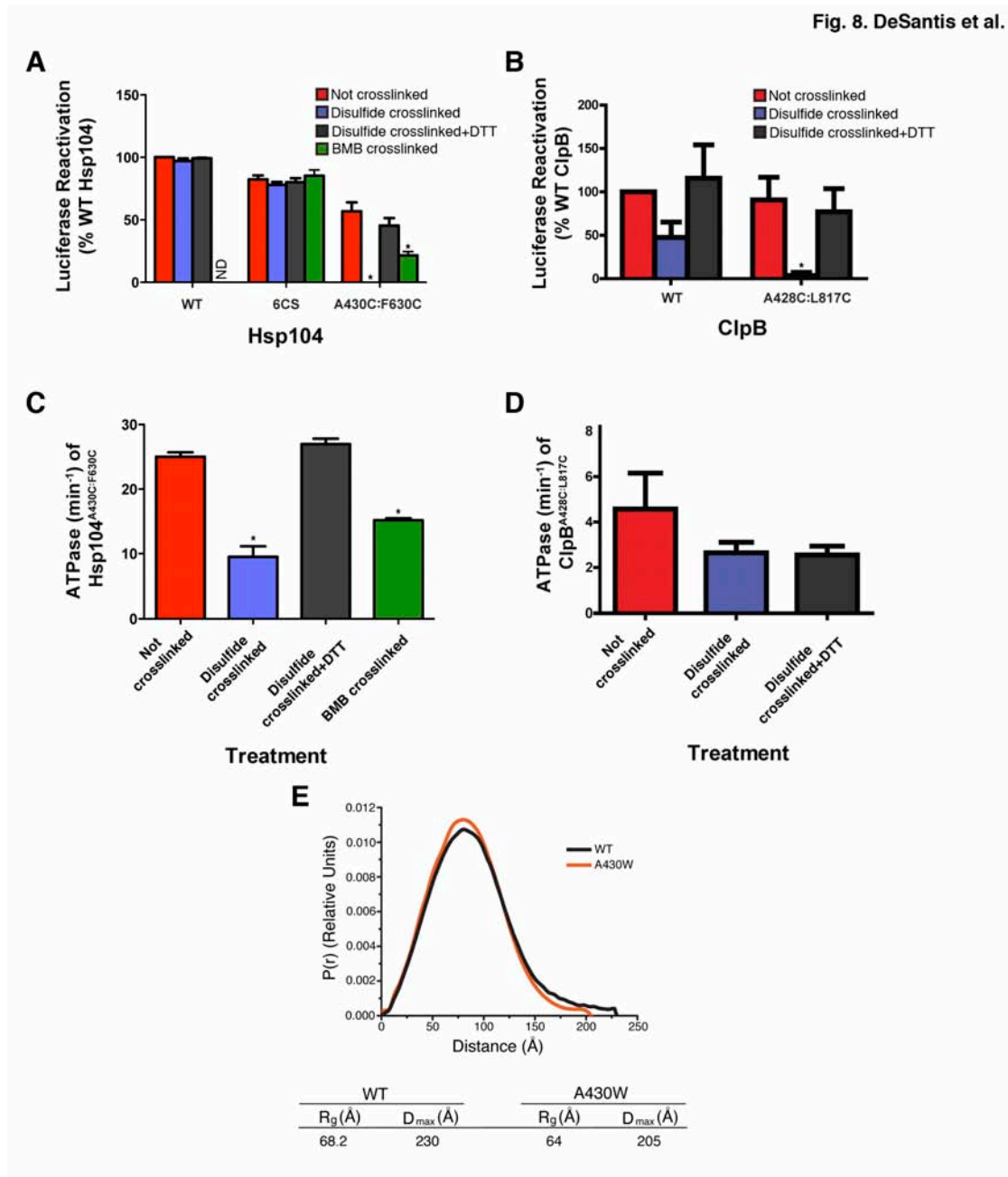


Figure 9

Fig. 9. DeSantis et al.

